Neuron

Article

Decoding neuronal composition and ontogeny of individual hypothalamic nuclei

Graphical Abstract

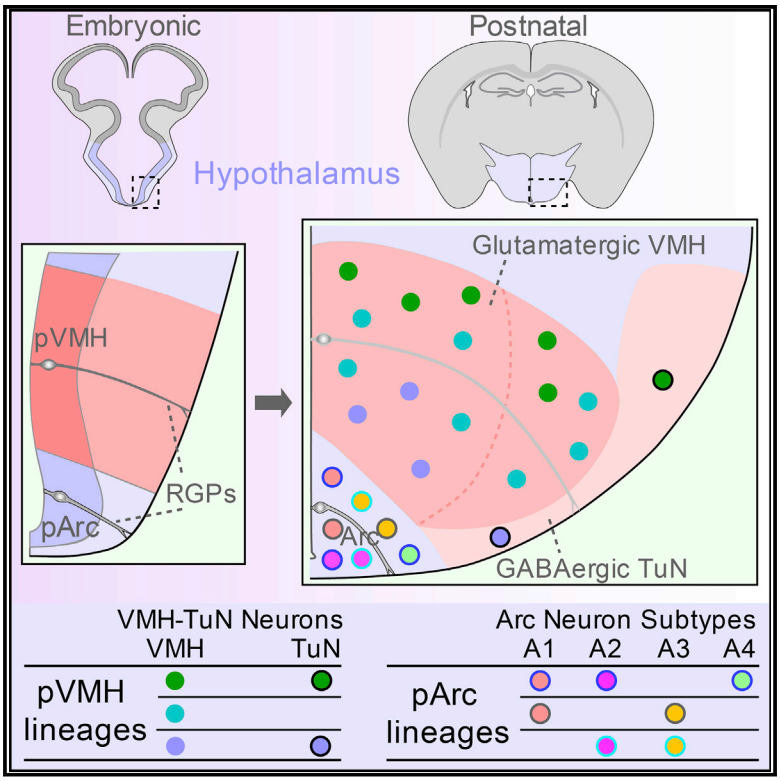

Highlights

- Combinatorial TF expression identifies all Arc, VMH, and TuN neurons
- All four subpopulations in the Arc are mosaically and simultaneously generated
- Glutamatergic VMH and GABAergic TuN neurons are generated from common progenitors
- Diverse lineages from individual radial glia progenitors build the Arc and VMH-TuN

Authors

Tong Ma, Samuel Zheng Hao Wong, Bora Lee, Guo-li Ming, Hongjun Song

Correspondence

shongjun@pennmedicine.upenn.edu

In Brief

The cellular mechanisms underlying development and organization of hypothalamic nuclei are poorly understood. Using transcription factor expression combinations and clonal lineage-tracing analysis, Ma et al. reveal that diverse lineages from multipotent radial glia progenitors establish neuronal diversity and orchestrate ontogenetic development of hypothalamic arcuate nucleus, ventromedial hypothalamus, and tuberal nucleus.

Ma et al., 2021, Neuron *109*, 1–18
April 7, 2021
https://doi.org/10.1016/j.neuron.2021.01.026

CellPress

Neuron

CellPress

Article

Decoding neuronal composition and ontogeny of individual hypothalamic nuclei

Tong Ma,[1] Samuel Zheng Hao Wong,[1,2] Bora Lee,[3] Guo-li Ming,[1,4,5,6] and Hongjun Song[1,4,5,7,8,*]
[1]Department of Neuroscience and Mahoney Institute for Neurosciences, Perelman School of Medicine, University of Pennsylvania, Philadelphia, PA 19104, USA
[2]The Cellular and Molecular Medicine Graduate Program, Johns Hopkins University School of Medicine, Baltimore, MD 21205, USA
[3]Center for Neuroscience, Korea Institute of Science and Technology, Seoul 02792, Korea
[4]Department of Cell and Developmental Biology, Perelman School of Medicine, University of Pennsylvania, Philadelphia, PA 19104, USA
[5]Institute for Regenerative Medicine, Perelman School of Medicine, University of Pennsylvania, Philadelphia, PA 19104, USA
[6]Department of Psychiatry, Perelman School of Medicine, University of Pennsylvania, Philadelphia, PA 19104, USA
[7]The Epigenetic Institute, Perelman School of Medicine, University of Pennsylvania, Philadelphia, PA 19104, USA
[8]Lead contact
*Correspondence: shongjun@pennmedicine.upenn.edu
https://doi.org/10.1016/j.neuron.2021.01.026

SUMMARY

The hypothalamus plays crucial roles in regulating endocrine, autonomic, and behavioral functions via its diverse nuclei and neuronal subtypes. The developmental mechanisms underlying ontogenetic establishment of different hypothalamic nuclei and generation of neuronal diversity remain largely unknown. Here, we show that combinatorial T-box 3 (TBX3), orthopedia homeobox (OTP), and distal-less homeobox (DLX) expression delineates all arcuate nucleus (Arc) neurons and defines four distinct subpopulations, whereas combinatorial NKX2.1/SF1 and OTP/DLX expression identifies ventromedial hypothalamus (VMH) and tuberal nucleus (TuN) neuronal subpopulations, respectively. Developmental analysis indicates that all four Arc subpopulations are mosaically and simultaneously generated from embryonic Arc progenitors, whereas glutamatergic VMH neurons and GABAergic TuN neurons are sequentially generated from common embryonic VMH progenitors. Moreover, clonal lineage-tracing analysis reveals that diverse lineages from multipotent radial glia progenitors orchestrate Arc and VMH-TuN establishment. Together, our study reveals cellular mechanisms underlying generation and organization of diverse neuronal subtypes and ontogenetic establishment of individual nuclei in the mammalian hypothalamus.

INTRODUCTION

The hypothalamus is an evolutionarily conserved structure that mediates essential homeostatic states and primitive behavioral functions, such as humoral control, sleep and circadian rhythms, feeding, energy balance, aggression, and sexual behavior (Saper and Lowell, 2014). Specific hypothalamic functions rely on numerous hypothalamic nuclei (or areas) and diverse neuronal subtypes (Markakis, 2002; Romanov et al., 2019; Saper and Lowell, 2014). The complete neuronal composition of individual hypothalamic nuclei and mechanisms underlying their ontogenetic establishment, however, remain largely unknown. Understanding the neuronal composition of brain structures and mechanisms underlying production and organization of diverse neuronal subtypes is a fundamental quest in neuroscience, which also facilitates the precise mapping of neuronal connectivity and dissection of specific behavioral circuits (Albright et al., 2000).

The hypothalamus is developmentally derived from the secondary prosencephalon in the context of the prosomeric model (Puelles et al., 2012). The embryonic hypothalamic area is patterned and regionalized into multiple progenitor domains, which have been characterized by specific combinations of molecular markers, notably transcription factors (TFs) (Bedont et al., 2015; Burbridge et al., 2016). How individual progenitor domains generate diverse neuronal subtypes and drive the formation of hypothalamic nuclei remain elusive. One major obstacle is a lack of specific and unique markers for comprehensively identifying and categorizing all neurons of individual hypothalamic nuclei. As an alternative strategy, combinatorial TF expression has been successfully applied to decipher various biological processes, particularly in neural development (Flames et al., 2007; Jessell, 2000). More importantly, compared to neuropeptides, which are usually used to identify different hypothalamic nuclei, the earlier expression of TFs during development can facilitate the study of neuronal subtype origins and nucleus establishment.

TFs play crucial roles in specification and production of neuronal subtypes in hypothalamic nuclei (Alvarez-Bolado, 2019; Bedont et al., 2015; Burbridge et al., 2016; Szarek et al., 2010; Xie and Dorsky, 2017). The arcuate nucleus (Arc) is composed of multiple discrete neuronal subtypes regulating

Please cite this article in press as: Ma et al., Decoding neuronal composition and ontogeny of individual hypothalamic nuclei, Neuron (2021), https://doi.org/10.1016/j.neuron.2021.01.026

feeding behavior and energy balance. TBX3 (T-box 3) is essential for differentiation of anorexigenic proopiomelanocortin (POMC) neurons and orexigenic neuropeptide Y (NPY)/agouti-related peptide (AgRP) neurons (Eriksson and Mignot, 2009; Quarta et al., 2019; Sanz et al., 2015). OTP (orthopedia homeobox) and DLX1/2 (distal-less homeobox 1/2) coordinate the generation of NPY/AgRP neurons and tyrosine hydroxylase (TH) neurons (Lee et al., 2018; Yee et al., 2009). The ventromedial hypothalamus (VMH) and the abutting tuberal nucleus (TuN) are situated adjacent to the Arc dorsally (Canteras et al., 1994; Kremer, 1992). The VMH, an essential region for energy homeostasis, aggression, and sexual behavior, is subdivided into dorsomedial (VMH_{dm}), central (VMH_c), and ventrolateral (VMH_{vl}) regions with different cellular architecture, anatomic projections, and molecular characterizations (Kurrasch et al., 2007; McClellan et al., 2006). SF1 (steroidogenic factor 1/NR5A1) specifically demarcates the postnatal $VMH_{dm/c}$ and determines the cytoarchitecture and neuronal distribution within the VMH (Cheung et al., 2013; Ikeda et al., 1995; McClellan et al., 2006; Shinoda et al., 1995; Tran et al., 2003). In contrast to the widely studied Arc and VMH, functions of the TuN are just beginning to be uncovered (Luo et al., 2018), and very little is known regarding its neuronal composition and development. Despite significant advances in functional studies and molecular analysis underlying neuron generation, cellular mechanisms underlying developmental establishment of the Arc, VMH, and TuN remain unknown.

Radial glia progenitors (RGPs) serve as neural precursors in the embryonic central nervous system (Kriegstein and Alvarez-Buylla, 2009), and individual RGP lineages have a critical role in establishing both laminar and nuclear brain structures, such as neocortex (Gao et al., 2014; Llorca et al., 2019) and thalamus (Shi et al., 2017; Wong et al., 2018). Previous studies have observed diverse dispersion patterns of individual lineages in the chick hypothalamic area (Arnold-Aldea and Cepko, 1996; Golden and Cepko, 1996). However, the role of individual RGP lineages in the developmental establishment of distinct mammalian hypothalamic nuclei remains unclear. Furthermore, given the diverse neuronal subtypes within individual hypothalamic nuclei, the lineage relationships among different neuronal subtypes remain to be investigated.

Here, we first identified a set of TF combinations to comprehensively characterize all neurons of Arc, VMH, and TuN and then applied these TF combinations to investigate the embryonic origin and developmental establishment of these nuclei. Through clonal lineage tracing, we uncovered the crucial role of individual RGP lineages in the production of diverse neuronal subtypes and ontogenetic establishment of the Arc, VMH, and TuN during development. Our findings reveal fundamental principles underlying the developmental establishment of hypothalamic nuclei and extend our understanding of cellular mechanisms that generate neuronal diversity.

RESULTS

Combinatorial TBX3, OTP, and DLX expression identifies all neurons in the Arc and defines four distinct subpopulations

To delineate neuronal composition in the Arc, we examined expression of different TFs (Figure 1A). Previous studies have shown that TBX3 (Eriksson and Mignot, 2009), OTP (Lee et al., 2018), and DLX (DLX1/DLX2 and DLX5/DLX6 bi-gene clusters are included herein; these genes are expressed in cells within the same lineage in the brain with DLX1/2 as upstream regulators of DLX5/6; Eisenstat et al., 1999; Yee et al., 2009) are each expressed by at least one neuronal subpopulation in the Arc. To identify DLX-lineage cells, we used DLX1/DLX2 antibodies and *DLX5/6-Cre* mice (Monory et al., 2006) crossed with nuclear-localized *H2B-GFP* reporter mice (He et al., 2012b) (hereafter, DLX^{GFP+} cells; Table S1). We validated that nearly all $DLX1^+$ (98%) and $DLX2^+$ cells (96%) contained DLX^{GFP} in the Arc at postnatal day 0 (P0) (n = 4; Figure S1A). About 73% and 90% of DLX^{GFP+} cells (n = 4) expressed DLX1 and DLX2, respectively, suggesting that DLX1 and DLX2 were downregulated in some DLX-lineage cells later. Triple immunostaining of TBX3, OTP, and DLX^{GFP} in P28 and P0 mice showed that each of these TFs labeled a subpopulation of Arc cells (Figures 1A–1C). TBX3 was also expressed in $vimentin^+$ tanycytes adjacent to the Arc (Figure S1B; Quarta et al., 2019). All $TBX3^+$, OTP^+, and DLX^{GFP+} cells in the Arc were $NeuN^+$ neurons (Figures 1D and S1C–S1E), and combinatorial expression of TBX3, OTP, and DLX^{GFP} labeled over 96% of all $NeuN^+$ Arc neurons (Figure 1D).

Combinatory TBX3, OTP, and DLX^{GFP} expression labels seven possible subpopulations (named Arc1–7 or A1–7; Figure 1E). At P28, more than 96% of TF^+ neurons belonged to Arc1–4 (Figure 1E). Arc5–7 had minor contributions to each of $TBX3^+$, OTP^+, and DLX^{GFP+} populations (Figure 1E, lower panel). Arc5–7 are rare because the vast majority of OTP^+ neurons expressed TBX3, and OTP^+ and DLX^{GFP+} neurons are non-overlapping populations in the Arc with only 3% of OTP^+ neurons containing DLX^{GFP} and 2% of DLX^{GFP+} neurons expressing OTP (n = 3; Figures 1B and 1C). Immunostaining confirmed that less than 1% of OTP^+ neurons expressed DLX1 and less than 2% of $DLX1^+$ neurons expressed OTP (n = 4; P0; Lee et al., 2018). Anatomically, Arc1 neurons were dispersed throughout the Arc; Arc2 neurons were mainly located in the ventromedial region of Arc (Arc_{vm}) with sparse distribution in the dorsomedial and ventrolateral regions of Arc (Arc_{dm} and Arc_{vl}); Arc3 neurons were observed throughout the Arc with the lowest density in the Arc_{vm}; and Arc4 neurons were mainly located in the Arc_{dm} and Arc_{vl} (Figures 1B, 1C, and 1F). We further confirmed that over 98% of $DLX2^+$ neurons contain DLX^{GFP} and about 90% of DLX^{GFP+} neurons express DLX2 at P28 (n = 3), and combinatorial TBX3, OTP, and DLX2 expression also delineated Arc1–4 subpopulations (Figures S1F–S1H). The similar proportions of Arc1–4 subpopulations identified by TBX3/OTP/DLX^{GFP} (Figure 1E) and TBX3/OTP/DLX2 (Figure S1G) suggest that DLX^{GFP} and DLX2 expression are largely interchangeable for delineating adult Arc1–4 subpopulations. Taken together, these results reveal that combinatorial TBX3, OTP, and DLX expression identifies nearly all Arc neurons and defines four major distinct neuronal subpopulations.

Arc subpopulations defined by TF combinations represent specific neuronal subtypes

Next, we systematically characterized TBX3, OTP, and DLX^{GFP} expression in functional neuronal subtypes, including POMC, NPY/AgRP, and TH neurons at P28 and P0. Nearly all $POMC^+$ neurons expressed TBX3 but rarely expressed OTP or DLX^{GFP}

Please cite this article in press as: Ma et al., Decoding neuronal composition and ontogeny of individual hypothalamic nuclei, Neuron (2021), https://doi.org/10.1016/j.neuron.2021.01.026

CellPress

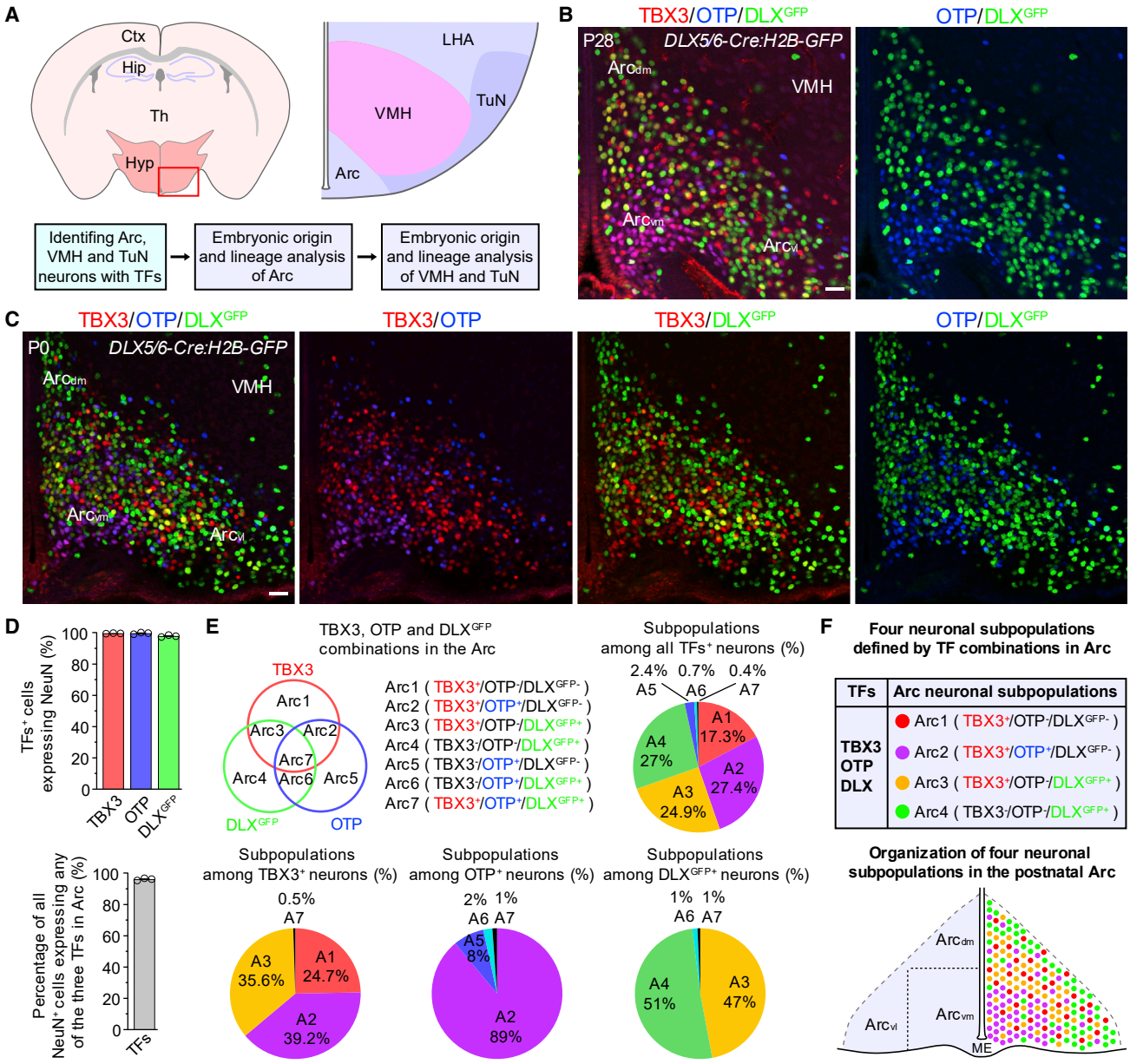

Figure 1. TBX3, OTP, and DLX^{GFP} combinations identify all Arc neurons and define four distinct neuronal subpopulations

(A) Schematic adult mouse forebrain coronal view with the hypothalamus (Hyp), arcuate nucleus (Arc), ventromedial hypothalamus (VMH), and tuberal nucleus (TuN) highlighted and experimental workflow. Ctx, cortex; Hip, hippocampus; LHA, lateral hypothalamic area; Th, thalamus.

(B and C) Sample confocal images of TBX3, OTP, and DLX^{GFP} expression in the Arc from *DLX5/6-Cre:H2B-GFP* mice at P28 (B) and P0 (C). Scale bars, 20 μm.

(D) Quantification of TBX3, OTP, DLX^{GFP}, and NeuN expression in the Arc. Values represent mean ± SEM (n = 3; P28).

(E) Schematic representation of possible neuronal subpopulations defined by combinatorial TBX3, OTP, and DLX^{GFP} expression in the Arc. Pie charts show percentages of neuronal subpopulations among specific populations. Values represent mean (n = 3; P28).

(F) Schematic summary of four major neuronal subpopulations and their organization in the postnatal Arc. ME, median eminence; dorsomedial (Arc$_{dm}$), ventrolateral (Arc$_{vl}$), and ventromedial (Arc$_{vm}$) regions of the Arc are shown.

See also Figure S1 and Table S1.

(Figures 2A and S2A). 87% of Arc1 (TBX3$^+$/OTP$^-$/DLX^{GFP-}) neurons expressed POMC, and 93% of POMC$^+$ neurons were Arc1 neurons (Figure 2B). To achieve better somatic labeling, NPY neurons were visualized by RNAscope fluorescent *in situ* hybridization at P28 (Figure 2C) and immunostaining at P0 (Figure S2B). Nearly all NPY neurons expressed TBX3 and OTP but rarely expressed DLX^{GFP} (Figures 2C and S2B). 85% of TBX3$^+$/OTP$^+$ neurons contained NPY, and 95% of NPY neurons were TBX3$^+$/OTP$^+$ (Figure 2D), which are almost the same population as TBX3$^+$/OTP$^+$/DLX^{GFP-} (Arc2) neurons, because nearly all OTP$^+$

Please cite this article in press as: Ma et al., Decoding neuronal composition and ontogeny of individual hypothalamic nuclei, Neuron (2021), https://doi.org/10.1016/j.neuron.2021.01.026

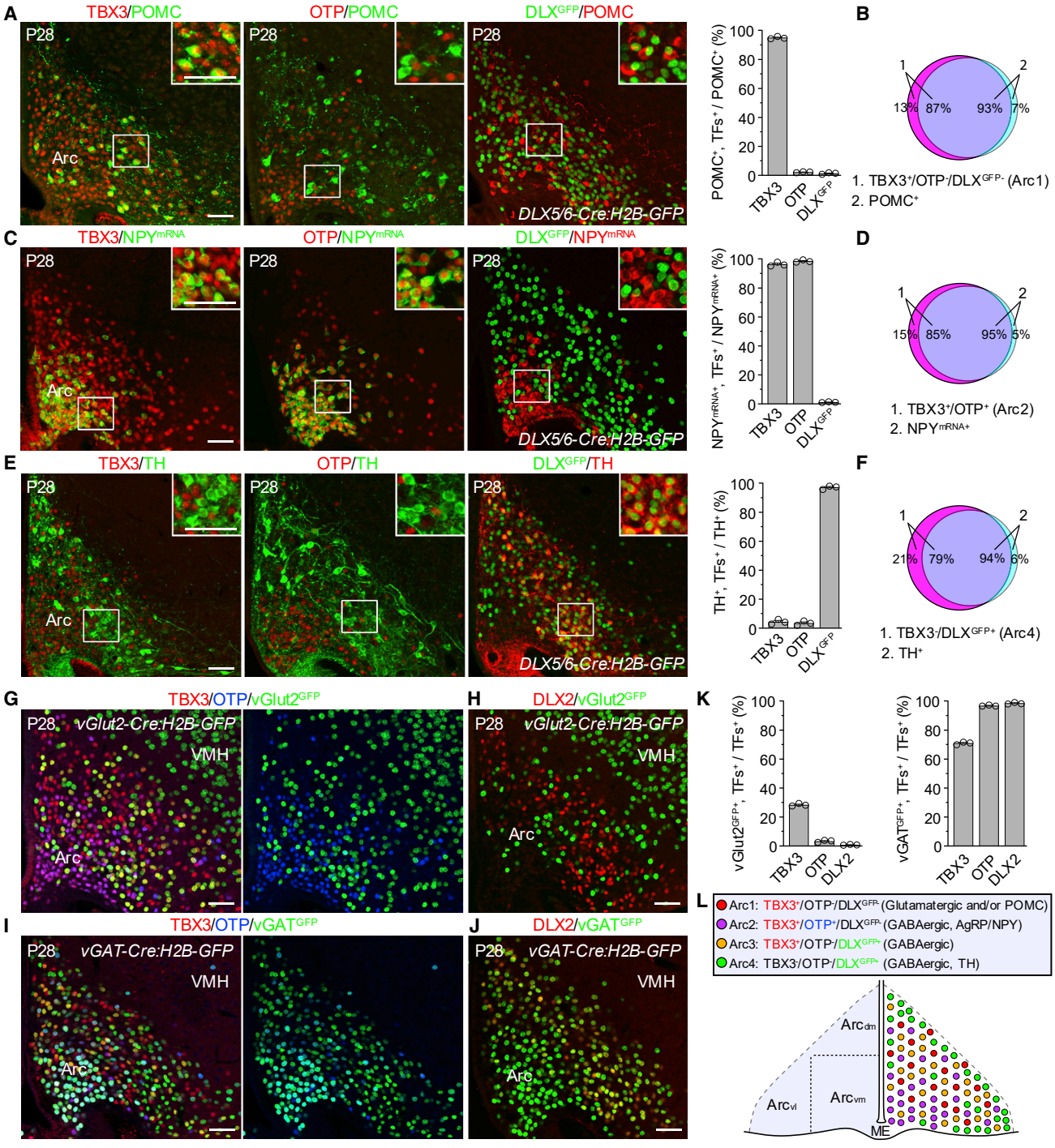

Figure 2. Neuronal subpopulations defined by TF combinations represent specific neuronal subtypes in the Arc

(A–F) Sample confocal images of POMC staining (A), NPY *in situ* (C), and TH staining (E), together with TBX3, OTP, and DLX^{GFP} staining in the Arc and quantification (B, D, and F). Scale bars, 50 μm. Values represent mean ± SEM (n = 3).

(G–K) Sample confocal images of TBX3, OTP, DLX2, and vGlut2^{GFP} (G and H) or vGAT^{GFP} (I and J) staining and quantifications (K). Scale bars, 50 μm. Values represent mean ± SEM (n = 3).

(L) Schematic summary of properties and organization of neuronal subpopulations defined by TF combinations in the Arc.

See also Figure S2.

Please cite this article in press as: Ma et al., Decoding neuronal composition and ontogeny of individual hypothalamic nuclei, Neuron (2021), https://doi.org/10.1016/j.neuron.2021.01.026

CellPress

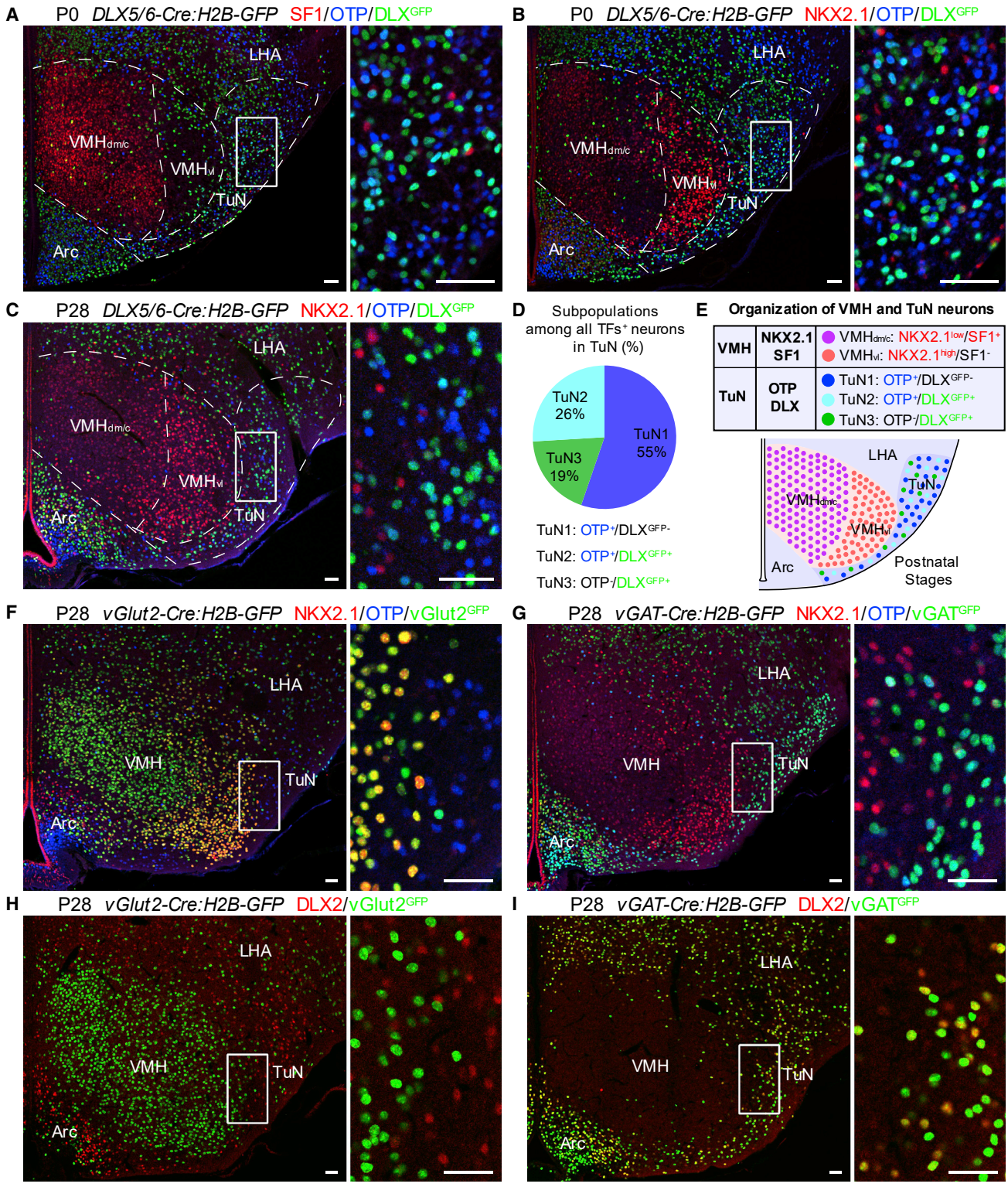

Figure 3. Molecular characterization of VMH and TuN neurons

(A–C) Sample confocal images of SF1, OTP, and DLX^{GFP} staining at P0 (A) and NKX2.1, OTP, and DLX^{GFP} staining at P0 (B) and P28 (C) in the VMH and TuN. Scale bars, 50 μm. Dorsomedial/central ($VMH_{dm/c}$) and ventromedial (VMH_{vl}) regions of the VMH are shown.

(D) Pie chart showing percentages of three neuronal subpopulations (TuN1–3) among all TF^{+} TuN neurons. Values represent mean (n = 3; P28).

(E) Schematic summary of molecular characterization and organization of VMH and TuN neurons.

(legend continued on next page)

Please cite this article in press as: Ma et al., Decoding neuronal composition and ontogeny of individual hypothalamic nuclei, Neuron (2021), https://doi.org/10.1016/j.neuron.2021.01.026

neurons are devoid of DLX^{GFP} in the Arc. Nearly all TH^+ neurons expressed DLX^{GFP} but rarely expressed TBX3 or OTP (Figures 2E and S2C). 79% of $TBX3^-/DLX^{GFP+}$ neurons expressed TH, and 94% of TH^+ neurons were $TBX3^-/DLX^{GFP+}$ (Figure 2F), which are almost the same population as $TBX3^-/OTP^-/DLX^{GFP+}$ (Arc4) neurons, because nearly all DLX^{GFP+} neurons are devoid of OTP in the Arc. We did not find a dominant functional marker expressed in Arc3 ($TBX3^+/OTP^-/DLX^{GFP+}$) neurons, which may be a heterogeneous population of GABAergic neurons (see below and discussion). Together, these results demonstrate that Arc1, Arc2, and Arc4 subpopulations defined by combinatorial TBX3, OTP, and DLX^{GFP} expression specifically represent POMC, NPY/AgRP, and TH neurons in the Arc, respectively.

To investigate glutamatergic and GABAergic phenotypes of TF^+ Arc neurons, we crossed *H2B-GFP* reporter mice with the *vGlut2-ires-Cre* or *vGAT-ires-Cre* knockin mice to label glutamatergic ($vGlut2^{GFP+}$) and GABAergic ($vGAT^{GFP+}$) neurons, respectively (Vong et al., 2011). Although 89% of $vGlut2^{GFP+}$ neurons expressed TBX3, only 28% of $TBX3^+$ neurons contained $vGlut2^{GFP}$ and nearly all OTP^+ and $DLX2^+$ neurons were devoid of $vGlut2^{GFP}$ (Figures 2G, 2H, 2K, S2D, S2E, and S2H). Hence, the majority of $vGlut2^{GFP+}$ neurons belong to Arc1 ($TBX3^+/OTP^-/DLX^{GFP-}$). In contrast, the majority of $TBX3^+$ neurons and nearly all OTP^+ and $DLX2^+$ neurons contained $vGAT^{GFP}$ (Figures 2I–2K and S2F–S2H). Thus, Arc2 ($TBX3^+/OTP^+/DLX^{GFP-}$), Arc3 ($TBX3^+/OTP^-/DLX^{GFP+}$), and Arc4 ($TBX3^-/OTP^-/DLX^{GFP+}$) neurons are GABAergic. We confirmed that a subpopulation (53%) of POMC neurons were glutamatergic, and nearly all NPY (NPY^{mRNA+}) and TH neurons were GABAergic (Figure S2I; Everitt et al., 1984; Ovesjö et al., 2001; Vong et al., 2011). These analyses show that all Arc2/NPY/AgRP, Arc3, and Arc4/TH neurons are GABAergic and a subpopulation of Arc1/POMC neurons are glutamatergic (Figure 2L).

To validate our molecular characterization of Arc neurons using TF combinations, we interrogated published single-cell transcriptome data of adult mouse Arc neurons (Campbell et al., 2017). Nine neuronal clusters (c0, c2, c3, c4, c6, c7, c10, c11, and c13) were identified among a total of 19 cell clusters (Figure S2J). The c4 cluster, representing 15% of all neurons, was identified as neurons from the neighboring VMH nucleus based on enrichment of NKX2.1, NR5A1 (SF1), and FEZF1 transcripts (Figure S2K; and see below; Campbell et al., 2017). The rest of the eight neuronal clusters, representing 85% of all neurons, were enriched in either TBX3, OTP, and/or DLX1/2/5/6 (Figure S2K). This is consistent with our result that TBX3, OTP, and DLX combinations identify nearly all Arc neurons. Specifically, the c2, c7, and c13 clusters belong to Arc1 ($TBX3^+/OTP^-/DLX^-$), including c2/POMC neurons. The c3 cluster represents Arc2 ($TBX3^+/OTP^+/DLX^-$)/NPY/AgRP neurons. The c6, c10, and c11 clusters belong to Arc4 ($TBX3^-/OTP^-/DLX^+$), including c6/TH and c10/TH neurons. In comparison, the c0 cluster is a much more heterogeneous population of GABAergic neurons, including Arc3 ($TBX3^+/OTP^-/DLX^+$; Figure S2K). Collectively, these analyses from single-cell transcriptome data confirmed that the TBX3, OTP, and DLX combinations delineate distinct Arc subpopulations.

NKX2.1/SF1 and OTP/DLX identify VMH and TuN neurons, respectively

Next, we investigated the VMH and TuN, which together are situated adjacent to the Arc dorsally (Figure 1A). Previous studies have shown that nearly all VMH neurons are derived from the SF1 lineage, but only $VMH_{dm/c}$ neurons persistently express SF1 at postnatal stages (Cheung et al., 2013). 69% of all $NeuN^+$ VMH neurons expressed SF1 at P28 (n = 3). $SF1^+$ VMH neurons rarely expressed OTP or DLX^{GFP} (<1%; n = 3; Figure 3A). Instead, NKX2.1 was expressed in all VMH subareas, with the highest expression in the VMH_{vl} (Figures 3B, 3C, and 3E; Correa et al., 2015). About 80% of all $NeuN^+$ VMH neurons expressed NKX2.1 (n = 3; Figure S3A). Less than 1.5% of $NKX2.1^+$ VMH neurons expressed OTP or DLX^{GFP} (n = 3; Figures 3B and 3C). NKX2.1 labels the majority of VMH neurons and can distinguish the VMH_{vl} from the $VMH_{dm/c}$ and the VMH from the lateral hypothalamus area (LHA) (Figures 3B and 3C).

We validated that 98% of $DLX2^+$ cells contained DLX^{GFP} and 88% of DLX^{GFP+} cells expressed DLX2 in the TuN (n = 4; P0). All OTP^+ and/or DLX^{GFP+} cells were $NeuN^+$ neurons, and combinations of OTP and DLX^{GFP} expression identified about 92% of all TuN neurons (n = 3; P28; Figure S3B). Systematic analysis revealed that three neuronal subpopulations defined by OTP and DLX^{GFP} combinations TuN1 (OTP^+/DLX^{GFP-}), TuN2 (OTP^+/DLX^{GFP+}), and TuN3 (OTP^-/DLX^{GFP+}) contributed 55%, 26%, and 19%, respectively (Figures 3D and 3E). Consistent with rare $SF1^+$ and $NKX2.1^+$ neurons in the TuN, there were few OTP^+ or DLX^{GFP+} neurons expressing SF1 or NKX2.1 ($\leq$2%; n = 3; Figures 3A–3C). We used the *SST-Cre:H2B-GFP* mice to label SST (somatostatin) neurons (Taniguchi et al., 2011), which have been found in the TuN (Luo et al., 2018). 93% of SST^{GFP+} neurons expressed OTP, whereas 63% of OTP^+ neurons contained SST^{GFP}, with few SST^{GFP+} neurons expressing DLX2 (7%; n = 3; Figures S3C and S3D). These results suggest that SST is preferentially expressed in TuN1 (OTP^+/DLX^{GFP-}) neurons.

Together, these results demonstrate that NKX2.1 identifies the majority of VMH neurons, and $NKX2.1^{low}/SF1^+$ and $NKX2.1^{high}/SF1^-$ delineate the $VMH_{dm/c}$ and VMH_{vl}, respectively (Figure 3E). Moreover, OTP and DLX^{GFP} combinations identify the vast majority of TuN neurons, define three subpopulations, and delineate TuN neurons from NKX2.1-labeled VMH neurons.

VMH and TuN neurons are glutamatergic and GABAergic, respectively

We found that 99% of $NKX2.1^+$ and $SF1^+$ neurons contained $vGlut2^{GFP}$, and less than 1% of $NKX2.1^+$ and $SF1^+$ neurons

(F and G) Sample confocal images showing that all $NKX2.1^+$ neurons of the VMH and rare OTP^+ neurons of the TuN contain $vGlut2^{GFP}$ (F) and rare $NKX2.1^+$ neurons of the VMH and all OTP^+ neurons of the TuN contain $vGAT^{GFP}$ (G). Scale bars, 50 μm.

(H and I) Sample confocal images showing that rare $DLX2^+$ cells of the TuN contain $vGlut2^{GFP}$ (H) and nearly all $DLX2^+$ cells of the TuN contain $vGAT^{GFP}$ (I). Scale bars, 50 μm.

See also Figure S3.

Please cite this article in press as: Ma et al., Decoding neuronal composition and ontogeny of individual hypothalamic nuclei, Neuron (2021), https://doi.org/10.1016/j.neuron.2021.01.026

contained vGAT^{GFP} (P28/P0; n = 3; Figures 3F, 3G, and S3E–S3H), consistent with VMH as a glutamatergic nucleus devoid of GABAergic neurons (Ovesjö et al., 2001; Vong et al., 2011; Ziegler et al., 2002). All NKX2.1^{+} neurons in the TuN, although rare, contained vGlut2^{GFP}, but not vGAT^{GFP} (Figures 3F, 3G, S3E, and S3F). Over 97% of all OTP^{+} and DLX2^{+} neurons in the TuN contained vGAT^{GFP}, but less than 2% contained vGlut2^{GFP} (P28/P0; n = 3; Figures 3F–3I, S3E, and S3F). All OTP^{+} and DLX2^{+} neurons in the VMH, although rare, contained vGAT^{GFP} but were devoid of vGlut2^{GFP} (Figures 3F–3I, S3E, and S3F). Together, these results indicate that nearly all VMH neurons are glutamatergic and nearly all TuN neurons are GABAergic.

Mosaic and simultaneous generation of diverse neuronal subpopulations in the embryonic Arc

We next applied the identified TF combinations to investigate developmental generation of neuronal diversity in hypothalamic nuclei. We first systematically investigated the TBX3, OTP, and DLX^{GFP} combinations in the embryonic Arc. TBX3 delineates a midline domain of the basal hypothalamic region, from which the presumptive Arc, median eminence, pituitary stalk, and posterior pituitary are derived (Pontecorvi et al., 2008; Quarta et al., 2019; Trowe et al., 2013). To distinguish it from other subdomains and the "Arc" nucleus, the subdomain of the TBX3^{+} progenitor region that gives rise to Arc neurons is referred to as "pArc" (progenitor domain of arcuate nucleus; Figure 4A).

Expression of TBX3, OTP, and DLX^{GFP} were analyzed at embryonic day 11.5 (E11.5), E12.5, E13.5, and E15.5. TBX3 was expressed in both progenitors of the pArc and many differentiating Arc neurons, whereas OTP and DLX^{GFP} were only expressed in differentiating neurons (Figures 4B and 4C). OTP^{+} and DLX^{GFP+} neurons were distributed in a mutually exclusive, salt-and-pepper pattern (Figures 4B and 4C). Although nearly all OTP^{+} neurons expressed TBX3, only a subpopulation of DLX^{GFP+} neurons expressed TBX3 (Figures 4B and 4C). Arc1–4 neurons could be identified as early as E11.5 (Figure 4B). The Arc1–3 neurons were intermingled together immediately adjacent to the pArc progenitors (Figures 4B and 4C), suggesting that they were generated from the common pArc domain. By contrast, the Arc4 neurons, the only TBX3^{-} subpopulation, were observed at the lateral edge of the presumptive Arc (Figures 4B and 4C). Considering that Arc4 neurons are also generated from the pArc progenitors (see clonal lineage-tracing results below), it is likely that they transiently expressed TBX3 before migrating away. Spatially segregated subdomains for Arc1–4 neurons were never observed throughout embryonic stages, suggesting that Arc1–4 subpopulations are mosaically generated from the common pArc domain. We further confirmed that about 94% of DLX2^{+} neurons express DLX^{GFP} and about 92% of DLX^{GFP+} neurons express DLX2 at E15.5 (n = 3), and Arc1–4 subpopulations and their mosaic generation were also identified with combinatorial TBX3, OTP, and DLX2 expression (Figure S4A).

To ascertain the establishment of distinct subpopulations in the embryonic Arc, we characterized the expression of POMC, NPY, and TH at E15.5, when a considerable number of these markers were observed. Nearly all POMC^{+} neurons expressed TBX3 but rarely OTP or DLX^{GFP} (Figure S4B), nearly all NPY^{+} neurons expressed TBX3 and OTP but rarely DLX^{GFP} (Figure S4C), and nearly all TH^{+} neurons contained DLX^{GFP} but rarely TBX3 or OTP (Figure S4D). These patterns of co-localization at E15.5 are consistent with those at P0 and P28 (Figures 2A–2F and S2). Thus, distinct Arc subpopulations are established at embryonic stages.

To confirm the simultaneous generation of Arc1–4 subpopulations in the embryonic Arc, we performed BrdU (bromodeoxyuridine) birth-dating analysis. Timed pregnant *DLX5/6-Cre:H2B-GFP* mice from E9.5 to E15.5 were given a single dose of BrdU, and brain samples were analyzed at P21. Quantification indicated that the vast majority of each Arc1–4 subpopulation were generated between E10.5 and E13.5 with a peak at E11.5/E12.5 (Figures 4D and 4E). Moreover, each Arc1–4 subpopulation was produced in similar proportions at a given time point (Figure 4E). Taken together, these results validated that Arc1–4 subpopulations are mosaically and simultaneously generated from the common pArc domain at embryonic stages, instead of being generated from spatially patterned progenitor subdomains.

Diverse lineages from multipotent pArc progenitors drive developmental Arc establishment

To further interrogate the cellular mechanism underlying the generation of neuronal diversity, we performed clonal lineage tracing using the Cre-mediated MADM (mosaic analysis with double markers) system (Hippenmeyer et al., 2010; Zong et al., 2005; Figure S5A; see STAR methods). To specifically and temporally label hypothalamic progenitors, we introduced the *Rax-CreER^{T2}* line into the MADM$^{GT/TG}$ system (Pak et al., 2014). In the embryonic hypothalamus, Rax was only expressed in progenitors of the ventricular zone, including the pArc domain as early as E9.5 (Lu et al., 2013; Figure S5B). We confirmed the reliability of the *Rax-CreER^{T2}* line with *Rax-CreER^{T2}:H2B-GFP* mice. A single dose of tamoxifen was administered to timed pregnant mice at E9.5, and brain samples were analyzed at E13.5. GFP^{+} progenitors and neurons were observed in the Arc, VMH, dorsomedial hypothalamus, paraventricular area (Pa), subparaventricular area (SPa), mammillary body area, median eminence, pituitary stalk, and posterior pituitary (Figure S5B; data not shown). No cells were labeled without tamoxifen administration (n = 5; P0 mice).

We injected a single dose of tamoxifen into timed pregnant *Rax-CreER^{T2}:MADM$^{GT/TG}$* mice at E9.5 and analyzed brains at E11.5/E12.5 for short-term tracing (Figure S5C). The dose of tamoxifen was optimized to achieve very sparse labeling, and serial sections were reconstructed to capture all labeled cells. Both green/red and yellow clones were observed in the hypothalamic area (Figures 5A and S5D). About 32% of hemispheres contained only one clone, and about 5% of them contained two or more clones in the hypothalamus (Figure 5B). The remaining hemispheres (63%) were devoid of any labeled cells in the hypothalamus.

To investigate features of individual hypothalamic progenitors, we specifically focused on green/red clones from G2-X events, which reveal the division pattern of original progenitors and their lineage potential (Bonaguidi et al., 2011; Gao et al., 2014; Zong et al., 2005). Among a total of 37 short-term (E9.5–E11.5/E12.5) green/red clones recovered in the hypothalamus, the

Please cite this article in press as: Ma et al., Decoding neuronal composition and ontogeny of individual hypothalamic nuclei, Neuron (2021), https://doi.org/10.1016/j.neuron.2021.01.026

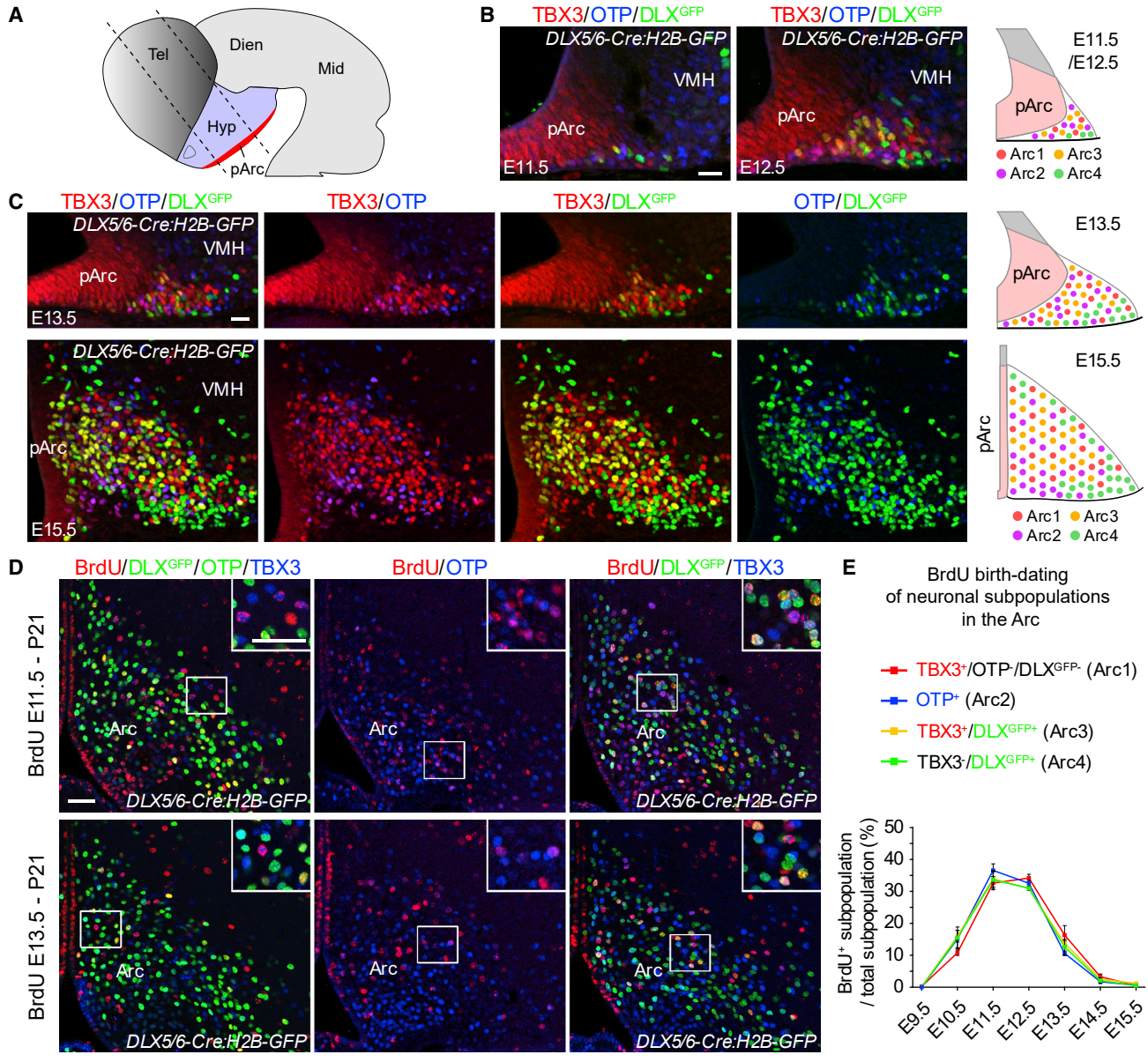

Figure 4. Mosaic and simultaneous generation of diverse neuronal subpopulations in the embryonic Arc

(A) Schematic drawing of the E11.5 neural tube with the hypothalamus (Hyp) and progenitor domain of Arc (pArc) highlighted. Dashed lines indicate sectioning orientation. Dien, diencephalon; Mid, midbrain; Tel, telencephalon.

(B and C) Sample confocal images of TBX3, OTP, and DLX^{GFP} staining and schematic drawings of the distribution of neuronal subpopulations in the embryonic Arc. Scale bars, 20 μm.

(D and E) Sample confocal images (D) and quantification (E) showing birth dating of neuronal subpopulations in the Arc. Scale bar, 50 μm. Values represent mean ± SEM (n = 3; P21).

See also Figure S4.

majority (65%) contained two RGPs (one green and one red and always close to each other; Figure 5A), indicating original symmetric division (Figure 5C). We also observed green/red clones with only one RGP^{G}/RGP^{R} accompanying certain (8% one/two and 5% more than two) red/green-differentiating cells (Figure S5E), indicating original asymmetric division (Figure 5C). In addition, clones with more than two RGPs (RGP^{G} and/or RGP^{R} having undergone proliferative symmetric division following the original division; 14%; Figures 5C and S5F) and a few clones without RGPs (only green and red differentiating cells; 8%; Figure S5G) were also observed.

To take advantage of some retained hypothalamic RGPs at P0 for position identification (Mirzadeh et al., 2017), we investigated P0 *Rax-CreER^{T2}:MADM$^{GT/TG}$* mice for long-term tracing

Please cite this article in press as: Ma et al., Decoding neuronal composition and ontogeny of individual hypothalamic nuclei, Neuron (2021), https://doi.org/10.1016/j.neuron.2021.01.026

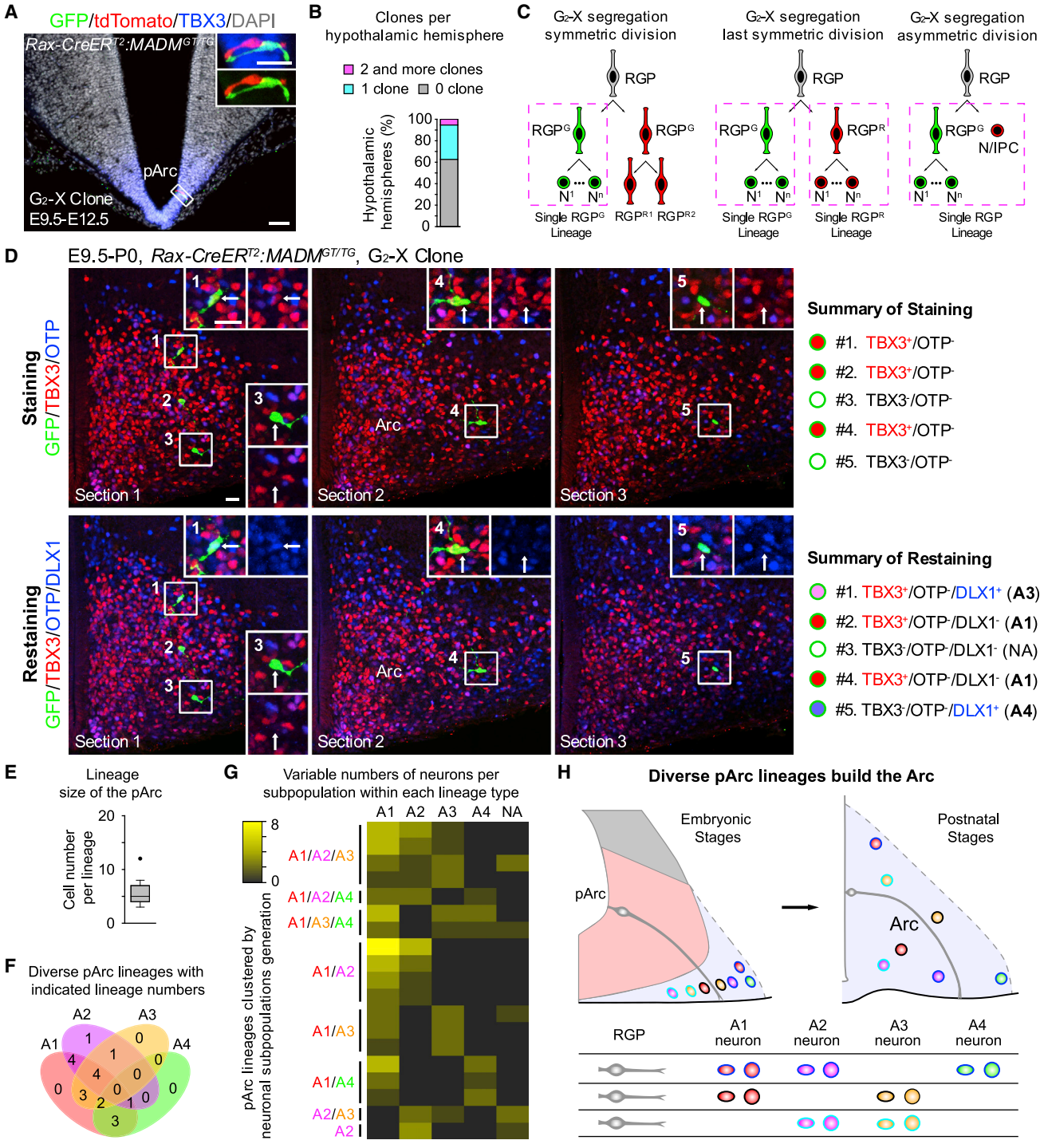

Figure 5. Diverse lineages from multipotent pArc progenitors drive developmental Arc establishment

(A) Sample confocal images of a short-term symmetric G_2-X clone in the embryonic Arc of the *Rax-CreER*^{T2}*:MADM*$^{GT/TG}$ mouse. Scale bars, 50 μm and 20 μm (magnified images).

(B) Summary of percentages of hemispheres with indicated numbers of clones in the hypothalamus (91 green/red and yellow clones from 212 hypothalamic hemispheres; E9.5–E11.5/E12.5).

(C) Schematic drawing showing symmetric division and asymmetric division of G_2-X segregation in the MADM$^{GT/TG}$ system. The complete lineages of individual RGPs are highlighted with purple rectangles. IPC, intermediate progenitor cell; N, neuron; RGP, radial glia progenitor.

(legend continued on next page)

Please cite this article in press as: Ma et al., Decoding neuronal composition and ontogeny of individual hypothalamic nuclei, Neuron (2021), https://doi.org/10.1016/j.neuron.2021.01.026

(Figure S5C). Because RGP^G and RGP^R lineages are equipotent in principle in the $MADM^{GT/TG}$ system, we only used the defined "complete individual RGP^G lineages" from the speculated symmetric division of G2-X events to analyze the individual pArc lineages (Figure 5C; see STAR methods). Because we used TBX3, OTP, and DLX combinations for Arc1–4 subpopulation identification and had limited available color channels, we developed a staining/restaining approach (Figure S5H; see STAR methods) for systematic analysis of neuronal production from individual pArc progenitors.

Among a total of 19 recovered complete individual RGP^G lineages of the Arc (E9.5–P0), 68% contained at least one retained RGP (RGP^G or RGP^R; Figure S5I). All neurons from individual RGP^G lineages with RGPs were restricted within the Arc, suggesting that pArc progenitors only generate Arc neurons. The RGP^G lineages had variable sizes containing 3–12 neurons (mean = 5; Figure 5E). The vast majority of RGP^G lineages consisted of two (58%) or three (37%) neuronal subpopulations, whereas 5% consisted of only one neuronal subpopulation and none consisted of all Arc1–4 subtypes (Figure 5F). The RGP^G lineages were surprisingly diverse with various lineage types corresponding to Arc1–4 combinations (Figure 5F). The numbers of neurons per subpopulation within each lineage were also highly variable (Figure 5G). Notably, some neurons from 26% of RGP^G lineages were devoid of TBX3, OTP, or DLX1 (NA in Figure 5G), consistent with downregulation of DLX1 in some DLX^{GFP+} neurons (Figure S1A) and the existence of rare $TBX3^-/OTP^-/DLX^{GFP-}$ Arc neurons (Figure 1D). The downregulation of DLX1 in some DLX^{GFP+} neurons, thus not detected by DLX1 antibodies, may lead to an underestimation of lineages containing DLX-lineage neurons and the lack of lineages consisting of all Arc1–4 subpopulations. Together, our results uncover that the pArc progenitors are multipotent and generate variable numbers of neurons with various combinations of Arc1–4 subpopulations to drive the developmental establishment of the Arc (Figure 5H).

Mosaic generation of glutamatergic VMH neurons and GABAergic TuN neurons from a common embryonic progenitor domain

To explore the embryonic development of the VMH and TuN, we first examined the expression of SF1 and OTP at embryonic stages. SF1 expression in the basal hypothalamus region was detected as early as E9.5 (Ikeda et al., 2001) and demarcated the presumptive VMH from E11.5 (Figure S6A). We refer to the progenitor region that gives rise to VMH neurons as "pVMH" (progenitor domain of VMH), which is adjacent to the pArc dorsally (Figures 6A and S6A). Surprisingly, sparse OTP^+ neurons also emerged from the pVMH and intermingled with SF^+ neurons in a mutually exclusive, salt-and-pepper pattern between E10.5 and E13.5 (Figures 6B and S6B). Moreover, OTP^+ neurons generated from the pVMH migrated laterally and accumulated in the presumptive TuN from E12.5 (Figures 6B and S6B).

NKX2.1 delineates the basal hypothalamic region, including the pVMH (Lu et al., 2013; Marín et al., 2002), and was found to be persistently expressed in many neurons (Figure 6C). Although rare OTP^+ neurons in the presumptive TuN expressed NKX2.1, many OTP^+ neurons adjacent to the pVMH progenitors expressed NKX2.1 at E12.5 (Figure 6C, upper panel), suggesting that OTP^+ neurons downregulated NKX2.1 expression while migrating laterally. Fate-mapping analysis using the *NKX2.1-Cre:H2B-GFP* mice (Xu et al., 2008) confirmed that nearly all OTP^+ neurons in the TuN contained $NKX2.1^{GFP}$ and thus were derived from the NKX2.1 lineage (P0/P28: 96%/97%; n = 3; Figure 6C, lower panel). Sparse $DLX2^+$ neurons were also generated from the pVMH, which migrated laterally, downregulated NKX2.1 expression, and accumulated in the presumptive TuN (Figure 6D, upper panel). Assessment of co-localization of DLX2 and $NKX2.1^{GFP}$ at P0 indicated that nearly all $DLX2^+$ TuN neurons were also derived from the NKX2.1 lineage (98%; n = 3; P0; Figure 6D, lower panel). Notably, the OTP/DLX-labeled TuN neurons, which were GABAergic (Figures 3G, 3I, and S3F) and derived from the NKX2.1 lineage (Figures 6C and 6D), were different from the OTP/DLX-labeled LHA neurons. OTP^+ LHA neurons were glutamatergic (Figures 3F and S3E) and generated from the paraventricular area (Wang and Lufkin, 2000), whereas DLX-labeled LHA neurons were GABAergic (Figure 3I) and generated from the subparaventricular area (Spa) (Figure 6D; Lu et al., 2013; Puelles et al., 2012). In addition, there were many OTP^+/DLX^{GFP+} cells (TuN2) in the TuN, but not in the LHA (Figures 3A–3C).

Given the glutamatergic identity of VMH neurons and GABAergic identity of TuN neurons at postnatal stages, it was unexpected that VMH and TuN neurons originate from a common pVMH domain. To provide more evidence of a common embryonic origin of glutamatergic and GABAergic neurons, we examined co-expression of SF1 or OTP with $vGlut2^{GFP}$ from *vGlut2-Cre:H2B-GFP* mice and $GAD2^{GFP}$ from *GAD2-Cre:H2B-GFP* mice (Taniguchi et al., 2011), which is expressed earlier in developing GABAergic neurons than $vGAT^{GFP}$ from *vGAT-Cre:H2B-GFP* mice at E12.5. In addition to large numbers of $SF1^+/vGlut2^{GFP+}$ VMH neurons (Figure S6C), we indeed

(D) Sample confocal images of an individual RGP^G lineage from a long-term symmetric G_2-X clone in the Arc. Cells from the RGP^R lineage were omitted (tdTomato not stained). The staining (upper panel)/restaining (lower panel) strategy was used to identify neuronal subpopulations of the Arc. Note that more blue cells can be observed after restaining. NA, not applicable. Scale bars, 50 μm and 20 μm (magnified images).

(E) Boxplot summarizing numbers of neurons in individual long-term RGP^G lineages (n = 19; RGP^G lineages; E9.5–P0). Center line, median; box, interquartile range; whiskers, minimum and maximum; individual points, outliers.

(F) Venn diagram summarizing diverse pArc lineages regarding Arc1–4 subpopulation generation (n = 19; RGP^G lineages; E9.5–P0). The numbers represent total lineages for each lineage type.

(G) Heatmap summarizing each neuronal subpopulation and their numbers generated from individual long-term RGP^G lineages (n = 19; E9.5–P0). Each row represents one RGP^G lineage.

(H) Model for the developmental establishment of the Arc. The multipotent pArc progenitors give rise to diverse lineages with various combinations of Arc1–4 subpopulations.

See also Figure S5.

Please cite this article in press as: Ma et al., Decoding neuronal composition and ontogeny of individual hypothalamic nuclei, Neuron (2021), https://doi.org/10.1016/j.neuron.2021.01.026

CellPress

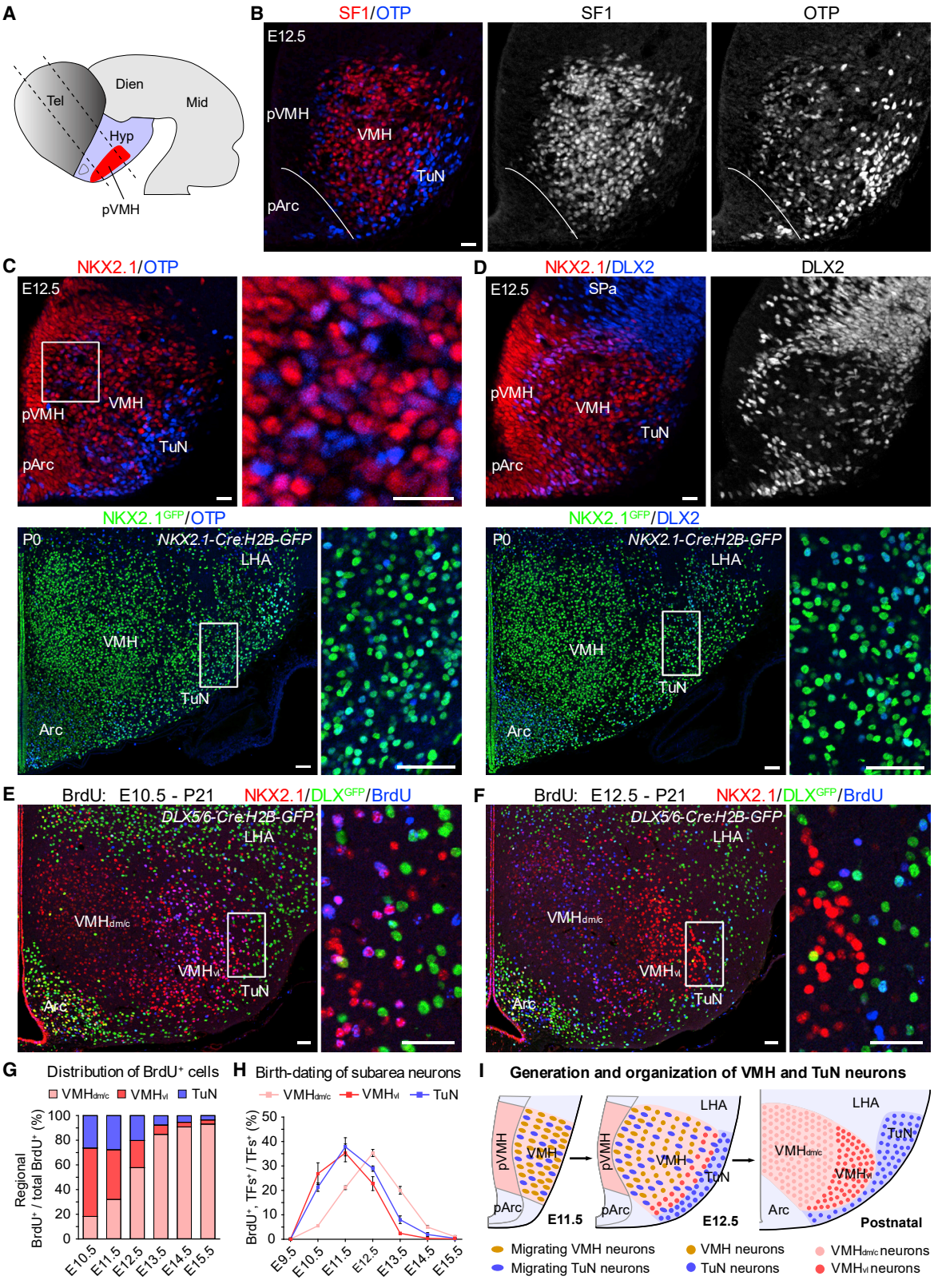

(legend on next page)

Please cite this article in press as: Ma et al., Decoding neuronal composition and ontogeny of individual hypothalamic nuclei, Neuron (2021), https://doi.org/10.1016/j.neuron.2021.01.026

observed that sparse OTP^{+}/GAD2^{GFP+} TuN neurons emerged from pVMH (Figure S6D).

Taken together, these results reveal that glutamatergic NKX2.1/SF1-labeled VMH neurons and GABAergic OTP/DLX-labeled TuN neurons are mosaically generated from a common embryonic pVMH domain, instead of spatially segregated progenitor subdomains.

Sequential and outside-in production of the VMH/TuN neurons

The common origin of VMH and TuN neurons from the pVMH suggests that the VMH-TuN has a laminar-like organization with $VMH_{dm/c}$, VMH_{vl}, and TuN subareas from medial to lateral, respectively, which can be delineated with low NKX2.1 expression in $VMH_{dm/c}$, high NKX2.1 expression in VMH_{vl}, and OTP/DLX^{GFP} expression in TuN. To investigate the timing of neuronal production in the VMH-TuN, timed pregnant *DLX5/6-Cre:H2B-GFP* mice from E9.5 to E15.5 were injected with a single pulse of BrdU and brain samples were examined at P21. Quantification of the distribution of BrdU^{+} cells generated at different times revealed that VMH-TuN neurons have a sequential and outside-in birth order, with early-born neurons mainly located in lateral subareas and late-born neurons in medial subareas (Figures 6E–6G). The vast majority of VMH_{vl} and TuN neurons were born between E10.5 and E12.5, with a peak at E11.5 (Figures 6E, 6F, 6H, S6E, and S6F). $VMH_{dm/c}$ neurons were mainly generated between E11.5 and E13.5, with a peak at E12.5 (Figures 6E, 6F, and 6H). Notably, the VMH_{vl} and TuN neurons were generated simultaneously (Figure 6H), consistent with the mosaic (salt-and-pepper) generation of the VMH and TuN neurons between E10.5 and E13.5 (Figures 6B and S6B). Together, these results reveal that the VMH-TuN as a whole has a laminar-like structure, and VMH-TuN neurons are produced in a sequential and outside-in histogenetic order (Figure 6I).

Diverse lineages from multipotent pVMH progenitors orchestrate VMH/TuN development

Finally, we investigated features of individual pVMH progenitors using the *Rax- CreER^{T2}:MADM$^{GT/TG}$* system (Figures S5B and 7A). We analyzed E9.5–E11.5/E12.5 clones for short-term tracing and E9.5–P0 clones for long-term tracing (Figure S5C). The generation of VMH neurons from pVMH progenitors was confirmed by SF1 staining with short-term clones (Figure 7B). Analysis of OTP expression using short-term and long-term clones with retained RGPs showed that pVMH progenitors indeed generated the OTP^{+} TuN neurons (Figures 7C and 7D).

We only used the defined "complete individual RGP^{G} lineages" from the speculated symmetric division of G2-X events to quantify the individual pVMH lineages for long-term tracing (E9.5–P0; Figure 5C). NKX2.1 and OTP were used to identify VMH and TuN neurons, respectively. The VMH-TuN subareas $VMH_{dm/c}$, VMH_{vl}, and TuN were delineated by coordinating the NKX2.1 expression level, OTP expression, and DAPI counterstaining (see STAR methods). Among a total of 30 recovered complete individual RGP^{G} lineages in the VMH-TuN, 67% retained at least one RGP (RGP^{G} or RGP^{R}; Figures 7D, S7A, and S7B). All neurons of individual pVMH lineages with RGPs were restricted within the VMH-TuN, suggesting that pVMH progenitors only generate VMH-TuN neurons. The neurons of individual pVMH lineages with or without RGPs exhibited various distribution patterns. About 40% of the lineages contained both VMH and TuN neurons (Figures 7D, 7F, and S7A), about 57% contained only VMH neurons (Figures 7E, 7F, and S7B), and 3% contained only TuN neurons (Figure 7F). The size of the lineages was highly variable, ranging from 1 to 13 neurons (mean = 6; Figure 7G). Although most neurons of individual lineages were distributed in the VMH, only one/two (or zero) neurons were usually observed in the TuN (Figure 7G). Analysis of the neuron distribution in VMH-TuN subareas $VMH_{dm/c}$, VMH_{vl}, and TuN showed that the majority of lineages (83%) was distributed in more than one subarea, with 27% of lineages distributed in all three subareas (Figure 7H). The distribution of individual lineages was very diverse, with various configurations of subarea distributions (Figure 7H). Moreover, the number of neurons in each subarea within each type of configuration was also highly variable (Figure 7I).

Together, these results reveal that the vast majority of pVMH progenitors are multipotent and generate variable numbers of neurons and multiple neuronal subpopulations, including glutamatergic VMH neurons and GABAergic TuN neurons, to orchestrate the development of the VMH and TuN (Figure 7J).

DISCUSSION

Using immunohistology and a large number of transgenic reporter mice, our study decoded the ontogenetic development of the hypothalamic Arc, VMH, and TuN (Figure 8A). Using combinatorial TBX3, OTP, and DLX expression analysis, we comprehensively identified all Arc neurons and defined four

Figure 6. Common embryonic origin and sequential generation of VMH and TuN neurons

(A) Schematic drawing of the E11.5 neural tube with the hypothalamus (Hyp) and progenitor domain of VMH (pVMH) highlighted. Dashed lines indicate the orientation of sectioning.

(B) Sample confocal images showing OTP^{+} and SF1^{+} neurons generated from the common pVMH at E12.5. Scale bar, 20 μm.

(C and D) Sample confocal images showing that OTP^{+} (C) and DLX2^{+} (D) neurons are generated from pVMH at E12.5, some of the OTP^{+} (C) and DLX2^{+} (D) neurons transiently express NKX2.1 (upper panel), and that nearly all OTP^{+} (C) and DLX2^{+} (D) neurons in TuN contain NKX2.1^{GFP} (P0; lower panel). Scale bars, 20 μm (upper panel) and 50 μm (lower panel).

(E and F) Sample confocal images showing distribution of BrdU^{+} cells in the VMH and TuN of P21 *DLX5/6-Cre:H2B-GFP* mice. BrdU was injected once at E10.5 (E) or E12.5 (F). Scale bars, 50 μm.

(G and H) Summaries of the regional distribution of BrdU^{+} cells generated at the indicated time point (G), and birth dating of neurons in specific regions (H). BrdU was injected once at indicated time points, and brain samples were analyzed at P21. Values represent mean ± SEM (n = 3).

(I) Schematic summary of the generation and organization of VMH and TuN neurons.

See also Figure S6.

Please cite this article in press as: Ma et al., Decoding neuronal composition and ontogeny of individual hypothalamic nuclei, Neuron (2021), https://doi.org/10.1016/j.neuron.2021.01.026

CellPress

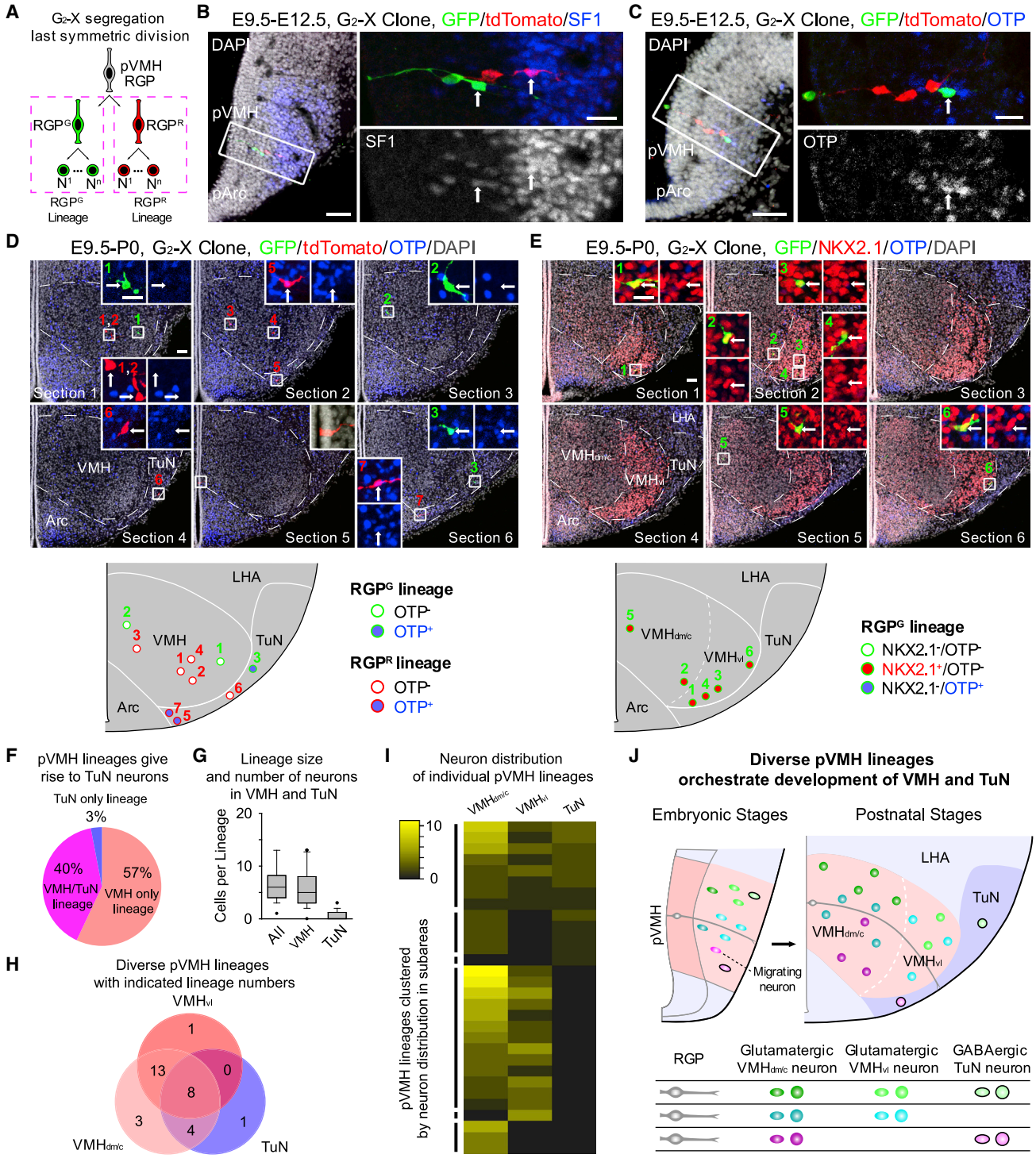

Figure 7. Diverse lineages from multipotent pVMH progenitors orchestrate VMH and TuN development

(A) Schematic drawing showing the last symmetric division of G_2-X segregation from pVMH progenitors with complete individual lineages highlighted with rectangles.

(B and C) Sample confocal images of short-term symmetric G_2-X clones from the pVMH of the *Rax-CreER^{T2}:MADM$^{GT/TG}$* mice. The pVMH progenitors can generate SF1$^+$ (B) and OTP$^+$ (C) neurons. Scale bars, 50 μm and 20 μm (magnified images).

(D) Sample confocal images of a long-term symmetric G_2-X clone from the pVMH (upper panel) and schematic drawing of the distribution and OTP expression of cells from the RGP^G and RGP^R lineages (lower panel). Both RGP^G and RGP^R lineages consist of VMH and TuN neurons. Note the retained RGP^R in section 5. Scale bars, 50 μm and 20 μm (magnified images).

(legend continued on next page)

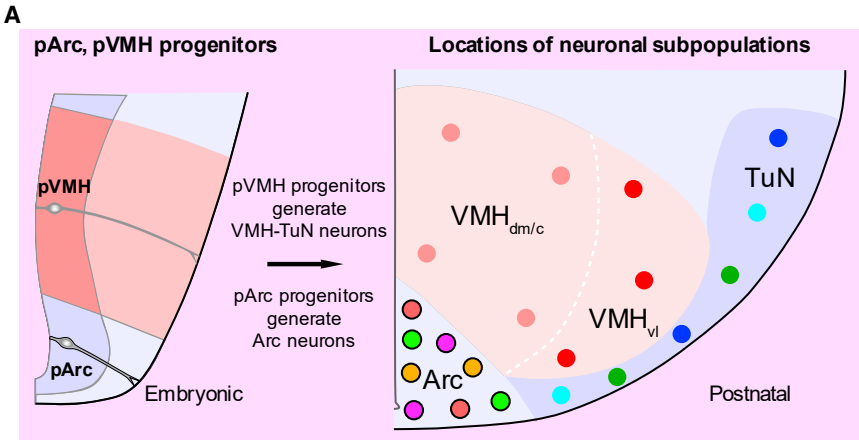

B

TFs of Nuclei		Neuronal Subpopulations
VMH	NKX2.1 SF1	VMH neuronal subpopulations $VMH_{dm/c}$: $NKX2.1^{low}$/$SF1^{+}$ VMH_{vl}: $NKX2.1^{high}$/$SF1^{-}$
TuN	OTP DLX	TuN neuronal subpopulations TuN1: OTP^{+}/DLX^{GFP-} TuN2: OTP^{+}/DLX^{GFP+} TuN3: OTP^{-}/DLX^{GFP+}
Arc	TBX3 OTP DLX	Arc neuronal subpopulations Arc1 ($TBX3^{+}$/OTP^{-}/DLX^{GFP-}) Arc2 ($TBX3^{+}$/OTP^{+}/DLX^{GFP-}) Arc3 ($TBX3^{+}$/OTP^{-}/DLX^{GFP+}) Arc4 ($TBX3^{-}$/OTP^{-}/DLX^{GFP+})

Figure 8. Schematic diagram of ontogenetic development and neuronal subpopulations of Arc and VMH-TuN

(A) Summary of ontogenetic establishment of Arc and VMH-TuN. The individual multipotent pArc and pVMH progenitors give rise to diverse neuronal subpopulations in Arc and VMH-TuN, respectively.

(B) Summary of neuronal composition in Arc and VMH-TuN defined with combinatory TF expression.

distinct subpopulations (Arc1–4; Figure 8B). We also characterized three TuN subpopulations (TuN1–3) with OTP and DLX^{GFP} combinations and delineated TuN neurons from abutting NKX2.1/SF1-labeled VMH neurons (Figure 8B). Using these TF combinations as tools, immunohistological analysis and BrdU birth dating demonstrated that four Arc subpopulations are mosaically and simultaneously generated from the pArc during embryonic stages, whereas, unexpectedly, glutamatergic VMH neurons and GABAergic TuN neurons are mosaically and sequentially generated from the common pVMH. MADM-based clonal lineage tracing further demonstrated diverse and highly variable lineages from multipotent pArc and pVMH progenitors. Collectively, these results reveal the complete neuronal composition of the Arc, VMH, and TuN and uncover the crucial role of individual RGP lineages in driving the formation of these nuclei. Our study provides a framework for studying and understanding neuronal composition, generation of neuronal diversity, and developmental establishment of individual hypothalamic nuclei and other complex brain structures.

Comprehensive characterization of neurons in hypothalamic nuclei with TF combinations

One reason for poor characterization of the neuronal composition of individual hypothalamic nuclei previously is the reliance on the expression of specific neuropeptides, which usually label only a neuronal subpopulation within individual nuclei (McClellan et al., 2006; Stuber and Wise, 2016; Swanson and Sawchenko, 1983). Recent applications of single-cell transcriptome analyses provide an advanced tool to comprehensively survey neuronal diversity of hypothalamic nuclei (Campbell et al., 2017; Chen et al., 2017; Mickelsen et al., 2019; Moffitt et al., 2018); however, it is challenging to use this approach to identify all neurons of individual nuclei with spatial and temporal information or to perform lineage analysis of individual progenitors. Future DNA barcoding followed with single-cell spatial transcriptome analysis may overcome these limitations (Weinreb et al., 2020). Our study suggests that TF combinations are a powerful tool for comprehensively identifying and spatially categorizing all neurons of individual hypothalamic nuclei. Nearly all Arc neurons and four discrete neuron subpopulations (Arc1–4) can be recognized by TBX3, OTP, and DLX combinations. The proportions of Arc1–4 subpopulations delineated by TBX3/OTP/DLX2 (Figure S1G) were consistent with the results from TBX3/OTP/DLX^{GFP} (Figure 1E) at the adult stage, suggesting that DLX2 expression is largely equivalent to Cre-dependent DLX^{GFP} expression for identifying adult Arc subpopulations. Importantly, the Arc1, Arc2, and Arc4 subpopulations mainly represent the functionally characterized POMC, NPY/AgRP, and TH neurons, respectively, which are consistent with previous immunohistological studies (Eriksson and Mignot, 2009; Lee et al., 2018;

(E) Sample confocal images of a long-term symmetric G_2-X clone from the pVMH (upper panel). Cells from the RGP^{R} lineage were omitted (tdTomato not stained). The schematic drawing summarizes the distribution and NKX2.1 and OTP expression of cells from the RGP^{G} lineage (lower panel). This RGP^{G} lineage consists of only VMH ($VMH_{dm/c}$ and VMH_{vl}) neurons. Scale bars, 50 μm and 20 μm (magnified images).

(F) Pie chart summarizing percentages of lineage types regarding VMH and TuN neuron generation (n = 30; RGP^{G} lineages; E9.5–P0).

(G) Boxplot summarizing numbers of total neurons, VMH neurons, and TuN neurons in individual RGP^{G} lineages (n = 30; E9.5–P0). Similar as in Figure 5E.

(H) Venn diagram summarizing pVMH lineage distribution in the $VMH_{dm/c}$, VMH_{vl}, and TuN (n = 30; RGP^{G} lineages; E9.5–P0). The numbers represent total lineages for each lineage type.

(I) Heatmap summarizing all pVMH lineages with neuron distribution in the $VMH_{dm/c}$, VMH_{vl}, and TuN (n = 30; RGP^{G} lineages; E9.5–P0). Each row represents one RGP^{G} lineage.

(J) Model for the developmental establishment of the VMH and TuN. The multipotent pVMH progenitors give rise to diverse lineages with various configurations of $VMH_{dm/c}$, VMH_{vl}, and TuN neurons to drive the developmental establishment of the VMH and TuN.

See also Figure S7.

Please cite this article in press as: Ma et al., Decoding neuronal composition and ontogeny of individual hypothalamic nuclei, Neuron (2021), https://doi.org/10.1016/j.neuron.2021.01.026

Sanz et al., 2015; Yee et al., 2009) and recent single-cell transcriptome analyses (Figure S2K; Campbell et al., 2017; Huisman et al., 2019). We note that the non-POMC, non-NPY/AgRP, and GABAergic characterizations of Arc3 neurons are similar to previously described RIP-Cre neurons, which sense leptin and drive energy expenditure (Campbell et al., 2017; Kong et al., 2012).

We showed that NKX2.1 labels both $SF1^+$ $VMH_{dm/c}$ neurons and VMH_{vl} neurons, and the OTP and DLX^{GFP} combinations identify the vast majority of TuN neurons and further define three TuN subpopulations (TuN1–3), including TuN1/SST neurons. Our results are consistent with previous findings that conditional knockout of NKX2.1 using the *SF1-Cre* line in the VMH decreases ERa and Tac1 neurons in the VMH_{vl} (Correa et al., 2015) and that SST neurons of the TuN are lost in the OTP mutant mice (Acampora et al., 1999). Given the crucial role of TuN1 (SST) neurons in regulating feeding behavior (Luo et al., 2018), our results raise the question of the functional significance of TuN2 and TuN3 neurons.

Spatiotemporal mechanisms of neuron production and organization in the hypothalamic nuclei

The embryonic hypothalamus is spatially patterned and subdivided into many distinct progenitor domains along rostro-caudal and dorso-ventral dimensions (Diez-Roux et al., 2011; Ferran et al., 2015; Shimogori et al., 2010). The relationships between individual progenitor domains and particular nuclei remain to be confirmed. Our results uncover the embryonic origin of Arc neurons from pArc and the common origin of VMH and TuN neurons from pVMH and corroborate the model that individual spatially patterned progenitor domains give rise to specific nuclei (Puelles et al., 2012). We also found that VMH-TuN neurons are generated in an outside-in temporal manner, consistent with previous observations (Shimada and Nakamura, 1973; Tran et al., 2003).

In the central nervous system, including the telencephalon (Marín and Müller, 2014), thalamus (Virolainen et al., 2012), brain stem (Gray, 2008), and spinal cord (Alaynick et al., 2011), glutamatergic and GABAergic neurons are mainly generated from distinct progenitor domains. However, generation of glutamatergic and GABAergic neurons from a common progenitor domain was observed in specific domains of the brain stem (Nakatani et al., 2007) and spinal cord (Cheng et al., 2004) at late embryonic stages. Our results demonstrated that both glutamatergic and GABAergic neurons are generated from the pArc and pVMH. Although glutamatergic and GABAergic neurons from the pArc intermingle within the Arc, those from the pVMH are segregated into the VMH and TuN. Importantly, our clonal analysis demonstrated that a single RGP can generate both glutamatergic and GABAergic neurons in the hypothalamus *in vivo*. Our findings thus reveal the diverse mechanisms underlying the production and organizational principle of glutamatergic and GABAergic neurons and provide insight into the developmental establishment of brain structures.

Features and lineage diversity of individual hypothalamic progenitors

Little is known about the role of individual hypothalamic progenitor lineages in the development of hypothalamic nuclei (Zhou et al., 2020). Taking advantage of the sparse MADM labeling system for clonal lineage analysis and TF combinations for neuronal subpopulation identification, our study revealed that the pArc progenitors are multipotent and can generate highly diverse lineage types consisting of various combinations of Arc1–4 subpopulations of different numbers. POMC, NPY/AgRP, and TH neurons are derived from the Arc1, Arc2, and Arc4 subpopulations, respectively, suggesting that individual pArc progenitors give rise to various combinations of POMC, NPY/AgRP, and TH neurons. About half of the individual pVMH progenitors generate both glutamatergic VMH neurons and GABAergic TuN neurons, whereas individual pVMH progenitors generating only TuN neurons were rarely observed, indicating that nearly all TuN neurons have a common origin with VMH neurons from individual pVMH progenitors. Our further analysis of neuron distribution indicated that the individual pVMH lineages are very diverse, and different lineage types comprise different configurations of the $VMH_{dm/c}$, VMH_{vl}, and TuN neurons. Our lineage analysis did not distinguish between VMH_{dm} and VMH_c and among TuN1–3, suggesting even more diverse lineage potentials. These results uncover that the vast majority of pVMH progenitors are multipotent progenitors, and the diverse lineages from the multipotent pVMH progenitors orchestrate the developmental establishment of the VMH and TuN.

Previous studies of the developing retina and neocortex suggested that multipotent neural progenitors progressively restricted their competence and sequentially generate different neuronal subtypes (Cepko, 2014; Kohwi and Doe, 2013). However, this classic competence model was challenged by recent studies, which suggested that individual neural progenitors subjected to stochastic factors give rise to diverse lineages with various combinations of neuronal subtypes (He et al., 2012a; Llorca et al., 2019). Our findings that diverse and variable lineages drive developmental establishment of the Arc and VMH-TuN resonate with these findings and raise the question of how pArc and pVMH progenitors achieve such a rich diversity of lineages. One possibility is that the RGPs are homogeneous and equipotent but behave heterogeneously and stochastically to generate diverse combinations of neuronal subtypes (He et al., 2012a). Another possibility is that the RGPs are heterogeneous and limited RGP types behave heterogeneously and stochastically to generate diverse combinations of neuronal subtypes (Llorca et al., 2019). It is also possible that multiple different RGP types with restricted potential generate specific combinations of neuronal subtypes (Franco et al., 2012). Future studies investigating the behaviors and molecular characterizations of the pArc and pVMH progenitors will uncover mechanisms underlying the lineage diversity.

In summary, our study uncovers the neuronal composition and ontogenetic establishment of the hypothalamic Arc, VMH, and TuN and highlights the power of TF combinations to study brain development and the critical role of individual progenitor lineages in generating neuronal diversity and orchestrating brain structure formation. Our study will also advance the investigation of hypothalamic development and provide insight into how diverse neuronal subtypes are produced and organized in the nervous system.

STAR★METHODS

Detailed methods are provided in the online version of this paper and include the following:

- KEY RESOURCES TABLE
- RESOURCE AVAILABILITY
  - Lead contact
  - Material availability
  - Data and code availability
- EXPERIMENTAL MODEL AND SUBJECT DETAILS
  - Animals
- METHOD DETAILS
  - BrdU and Tamoxifen Treatments
  - Brain Tissue Preparation and Sectioning
  - Immunohistology, Confocal Imaging and Counting
  - Antigen Retrieval Treatment
  - *In Situ* Hybridization
  - Single-cell RNA Sequencing Analysis
  - MADM-based Clonal Lineage Analyses
  - Staining/Restaining Protocol
- QUANTIFICATION AND STATISTICAL ANALYSIS
  - Quantification of Population-Level Analyses
  - BrdU Birth-Dating Analysis

SUPPLEMENTAL INFORMATION

Supplemental Information can be found online at https://doi.org/10.1016/j.neuron.2021.01.026.

ACKNOWLEDGMENTS

We thank members of Ming and Song laboratories for suggestions, B. Temsamrit and E. LaNoce for technical support, J. Schnoll for lab coordination, Z. Josh Huang for *H2B-GFP* reporter mice, Zhengang Yang for DLX2 antibodies, and Jae W. Lee for Dlx1 antibodies. This work was supported by grants from National Institutes of Health (R35NS116843 and P01NS097206 to H.S. and R35NS097370 to G.M.).

AUTHOR CONTRIBUTIONS

T.M. contributed to all aspects of the project. S.Z.H.W. contributed to additional data collection. B.L. contributed reagents. T.M., G.M., and H.S. conceived the project and wrote the manuscript.

DECLARATION OF INTERESTS

H.S. is a member of the advisory board for *Neuron*. The authors declare no other competing interests.

Received: June 14, 2020
Revised: October 10, 2020
Accepted: January 26, 2021
Published: February 17, 2021

REFERENCES

Acampora, D., Postiglione, M.P., Avantaggiato, V., Di Bonito, M., Vaccarino, F.M., Michaud, J., and Simeone, A. (1999). Progressive impairment of developing neuroendocrine cell lineages in the hypothalamus of mice lacking the Orthopedia gene. Genes Dev. *13*, 2787–2800.

Alaynick, W.A., Jessell, T.M., and Pfaff, S.L. (2011). SnapShot: spinal cord development. Cell *146*, 178–178.e1.

Albright, T.D., Jessell, T.M., Kandel, E.R., and Posner, M.I. (2000). Neural science: a century of progress and the mysteries that remain. Cell *100* (*Suppl*), S1–S55.

Alvarez-Bolado, G. (2019). Development of neuroendocrine neurons in the mammalian hypothalamus. Cell Tissue Res. *375*, 23–39.

Arnold-Aldea, S.A., and Cepko, C.L. (1996). Dispersion patterns of clonally related cells during development of the hypothalamus. Dev. Biol. *173*, 148–161.

Babicki, S., Arndt, D., Marcu, A., Liang, Y., Grant, J.R., Maciejewski, A., and Wishart, D.S. (2016). Heatmapper: web-enabled heat mapping for all. Nucleic Acids Res. *44* (W1), W147–W153.

Bedont, J.L., Newman, E.A., and Blackshaw, S. (2015). Patterning, specification, and differentiation in the developing hypothalamus. Wiley Interdiscip. Rev. Dev. Biol. *4*, 445–468.

Berg, D.A., Su, Y., Jimenez-Cyrus, D., Patel, A., Huang, N., Morizet, D., Lee, S., Shah, R., Ringeling, F.R., Jain, R., et al. (2019). A common embryonic origin of stem cells drives developmental and adult neurogenesis. Cell *177*, 654–668.e15.

Bonaguidi, M.A., Wheeler, M.A., Shapiro, J.S., Stadel, R.P., Sun, G.J., Ming, G.L., and Song, H. (2011). In vivo clonal analysis reveals self-renewing and multipotent adult neural stem cell characteristics. Cell *145*, 1142–1155.

Burbridge, S., Stewart, I., and Placzek, M. (2016). Development of the neuroendocrine hypothalamus. Compr. Physiol. *6*, 623–643.

Butler, A., Hoffman, P., Smibert, P., Papalexi, E., and Satija, R. (2018). Integrating single-cell transcriptomic data across different conditions, technologies, and species. Nat. Biotechnol. *36*, 411–420.

Campbell, J.N., Macosko, E.Z., Fenselau, H., Pers, T.H., Lyubetskaya, A., Tenen, D., Goldman, M., Verstegen, A.M., Resch, J.M., McCarroll, S.A., et al. (2017). A molecular census of arcuate hypothalamus and median eminence cell types. Nat. Neurosci. *20*, 484–496.

Canteras, N.S., Simerly, R.B., and Swanson, L.W. (1994). Organization of projections from the ventromedial nucleus of the hypothalamus: a Phaseolus vulgaris-leucoagglutinin study in the rat. J. Comp. Neurol. *348*, 41–79.

Cepko, C. (2014). Intrinsically different retinal progenitor cells produce specific types of progeny. Nat. Rev. Neurosci. *15*, 615–627.

Chen, R., Wu, X., Jiang, L., and Zhang, Y. (2017). Single-cell RNA-seq reveals hypothalamic cell diversity. Cell Rep. *18*, 3227–3241.

Cheng, L., Arata, A., Mizuguchi, R., Qian, Y., Karunaratne, A., Gray, P.A., Arata, S., Shirasawa, S., Bouchard, M., Luo, P., et al. (2004). Tlx3 and Tlx1 are post-mitotic selector genes determining glutamatergic over GABAergic cell fates. Nat. Neurosci. *7*, 510–517.

Cheung, C.C., Kurrasch, D.M., Liang, J.K., and Ingraham, H.A. (2013). Genetic labeling of steroidogenic factor-1 (SF-1) neurons in mice reveals ventromedial nucleus of the hypothalamus (VMH) circuitry beginning at neurogenesis and development of a separate non-SF-1 neuronal cluster in the ventrolateral VMH. J. Comp. Neurol. *521*, 1268–1288.

Correa, S.M., Newstrom, D.W., Warne, J.P., Flandin, P., Cheung, C.C., Lin-Moore, A.T., Pierce, A.A., Xu, A.W., Rubenstein, J.L., and Ingraham, H.A. (2015). An estrogen-responsive module in the ventromedial hypothalamus selectively drives sex-specific activity in females. Cell Rep. *10*, 62–74.

Diez-Roux, G., Banfi, S., Sultan, M., Geffers, L., Anand, S., Rozado, D., Magen, A., Canidio, E., Pagani, M., Peluso, I., et al. (2011). A high-resolution anatomical atlas of the transcriptome in the mouse embryo. PLoS Biol. *9*, e1000582.

Eisenstat, D.D., Liu, J.K., Mione, M., Zhong, W., Yu, G., Anderson, S.A., Ghattas, I., Puelles, L., and Rubenstein, J.L. (1999). DLX-1, DLX-2, and DLX-5 expression define distinct stages of basal forebrain differentiation. J. Comp. Neurol. *414*, 217–237.

Eriksson, K.S., and Mignot, E. (2009). T-box 3 is expressed in the adult mouse hypothalamus and medulla. Brain Res. *1302*, 233–239.

Everitt, B.J., Hökfelt, T., Wu, J.Y., and Goldstein, M. (1984). Coexistence of tyrosine hydroxylase-like and gamma-aminobutyric acid-like immunoreactivities in neurons of the arcuate nucleus. Neuroendocrinology *39*, 189–191.

Ferran, J.L., Puelles, L., and Rubenstein, J.L. (2015). Molecular codes defining rostrocaudal domains in the embryonic mouse hypothalamus. Front. Neuroanat. *9*, 46.

Flames, N., Pla, R., Gelman, D.M., Rubenstein, J.L., Puelles, L., and Marín, O. (2007). Delineation of multiple subpallial progenitor domains by the combinatorial expression of transcriptional codes. J. Neurosci. *27*, 9682–9695.

Franco, S.J., Gil-Sanz, C., Martinez-Garay, I., Espinosa, A., Harkins-Perry, S.R., Ramos, C., and Müller, U. (2012). Fate-restricted neural progenitors in the mammalian cerebral cortex. Science *337*, 746–749.

Gao, P., Postiglione, M.P., Krieger, T.G., Hernandez, L., Wang, C., Han, Z., Streicher, C., Papusheva, E., Insolera, R., Chugh, K., et al. (2014). Deterministic progenitor behavior and unitary production of neurons in the neocortex. Cell *159*, 775–788.

Golden, J.A., and Cepko, C.L. (1996). Clones in the chick diencephalon contain multiple cell types and siblings are widely dispersed. Development *122*, 65–78.

Gray, P.A. (2008). Transcription factors and the genetic organization of brain stem respiratory neurons. J. Appl. Physiol. (1985) *104*, 1513–1521.

He, J., Zhang, G., Almeida, A.D., Cayouette, M., Simons, B.D., and Harris, W.A. (2012a). How variable clones build an invariant retina. Neuron *75*, 786–798.

He, M., Liu, Y., Wang, X., Zhang, M.Q., Hannon, G.J., and Huang, Z.J. (2012b). Cell-type-based analysis of microRNA profiles in the mouse brain. Neuron *73*, 35–48.

Hippenmeyer, S., Youn, Y.H., Moon, H.M., Miyamichi, K., Zong, H., Wynshaw-Boris, A., and Luo, L. (2010). Genetic mosaic dissection of Lis1 and Ndel1 in neuronal migration. Neuron *68*, 695–709.

Huisman, C., Cho, H., Brock, O., Lim, S.J., Youn, S.M., Park, Y., Kim, S., Lee, S.K., Delogu, A., and Lee, J.W. (2019). Single cell transcriptome analysis of developing arcuate nucleus neurons uncovers their key developmental regulators. Nat. Commun. *10*, 3696.

Ikeda, Y., Luo, X., Abbud, R., Nilson, J.H., and Parker, K.L. (1995). The nuclear receptor steroidogenic factor 1 is essential for the formation of the ventromedial hypothalamic nucleus. Mol. Endocrinol. *9*, 478–486.

Ikeda, Y., Takeda, Y., Shikayama, T., Mukai, T., Hisano, S., and Morohashi, K.I. (2001). Comparative localization of Dax-1 and Ad4BP/SF-1 during development of the hypothalamic-pituitary-gonadal axis suggests their closely related and distinct functions. Dev. Dyn. *220*, 363–376.

Jessell, T.M. (2000). Neuronal specification in the spinal cord: inductive signals and transcriptional codes. Nat. Rev. Genet. *1*, 20–29.

Kohwi, M., and Doe, C.Q. (2013). Temporal fate specification and neural progenitor competence during development. Nat. Rev. Neurosci. *14*, 823–838.

Kong, D., Tong, Q., Ye, C., Koda, S., Fuller, P.M., Krashes, M.J., Vong, L., Ray, R.S., Olson, D.P., and Lowell, B.B. (2012). GABAergic RIP-Cre neurons in the arcuate nucleus selectively regulate energy expenditure. Cell *151*, 645–657.

Kremer, H.P. (1992). The hypothalamic lateral tuberal nucleus: normal anatomy and changes in neurological diseases. Prog. Brain Res. *93*, 249–261.

Kriegstein, A., and Alvarez-Buylla, A. (2009). The glial nature of embryonic and adult neural stem cells. Annu. Rev. Neurosci. *32*, 149–184.

Kurrasch, D.M., Cheung, C.C., Lee, F.Y., Tran, P.V., Hata, K., and Ingraham, H.A. (2007). The neonatal ventromedial hypothalamus transcriptome reveals novel markers with spatially distinct patterning. J. Neurosci. *27*, 13624–13634.

Kuwajima, T., Nishimura, I., and Yoshikawa, K. (2006). Necdin promotes GABAergic neuron differentiation in cooperation with Dlx homeodomain proteins. J Neurosci *26*, 5383–5392.

Lee, B., Kim, J., An, T., Kim, S., Patel, E.M., Raber, J., Lee, S.K., Lee, S., and Lee, J.W. (2018). Dlx1/2 and Otp coordinate the production of hypothalamic GHRH- and AgRP-neurons. Nat. Commun. *9*, 2026.

Llorca, A., Ciceri, G., Beattie, R., Wong, F.K., Diana, G., Serafeimidou-Pouliou, E., Fernández-Otero, M., Streicher, C., Arnold, S.J., Meyer, M., et al. (2019). A stochastic framework of neurogenesis underlies the assembly of neocortical cytoarchitecture. eLife *8*, e51381.

Lu, F., Kar, D., Gruenig, N., Zhang, Z.W., Cousins, N., Rodgers, H.M., Swindell, E.C., Jamrich, M., Schuurmans, C., Mathers, P.H., and Kurrasch, D.M. (2013). Rax is a selector gene for mediobasal hypothalamic cell types. J. Neurosci. *33*, 259–272.

Luo, S.X., Huang, J., Li, Q., Mohammad, H., Lee, C.Y., Krishna, K., Kok, A.M., Tan, Y.L., Lim, J.Y., Li, H., et al. (2018). Regulation of feeding by somatostatin neurons in the tuberal nucleus. Science *361*, 76–81.

Marín, O., and Müller, U. (2014). Lineage origins of GABAergic versus glutamatergic neurons in the neocortex. Curr. Opin. Neurobiol. *26*, 132–141.

Marín, O., Baker, J., Puelles, L., and Rubenstein, J.L. (2002). Patterning of the basal telencephalon and hypothalamus is essential for guidance of cortical projections. Development *129*, 761–773.

Markakis, E.A. (2002). Development of the neuroendocrine hypothalamus. Front. Neuroendocrinol. *23*, 257–291.

McClellan, K.M., Parker, K.L., and Tobet, S. (2006). Development of the ventromedial nucleus of the hypothalamus. Front. Neuroendocrinol. *27*, 193–209.

Mickelsen, L.E., Bolisetty, M., Chimileski, B.R., Fujita, A., Beltrami, E.J., Costanzo, J.T., Naparstek, J.R., Robson, P., and Jackson, A.C. (2019). Single-cell transcriptomic analysis of the lateral hypothalamic area reveals molecularly distinct populations of inhibitory and excitatory neurons. Nat. Neurosci. *22*, 642–656.

Mirzadeh, Z., Kusne, Y., Duran-Moreno, M., Cabrales, E., Gil-Perotin, S., Ortiz, C., Chen, B., Garcia-Verdugo, J.M., Sanai, N., and Alvarez-Buylla, A. (2017). Bi- and uniciliated ependymal cells define continuous floor-plate-derived tanycytic territories. Nat. Commun. *8*, 13759.

Moffitt, J.R., Bambah-Mukku, D., Eichhorn, S.W., Vaughn, E., Shekhar, K., Perez, J.D., Rubinstein, N.D., Hao, J., Regev, A., Dulac, C., and Zhuang, X. (2018). Molecular, spatial, and functional single-cell profiling of the hypothalamic preoptic region. Science *362*, eaau5324.

Monory, K., Massa, F., Egertová, M., Eder, M., Blaudzun, H., Westenbroek, R., Kelsch, W., Jacob, W., Marsch, R., Ekker, M., et al. (2006). The endocannabinoid system controls key epileptogenic circuits in the hippocampus. Neuron *51*, 455–466.

Nakatani, T., Minaki, Y., Kumai, M., and Ono, Y. (2007). Helt determines GABAergic over glutamatergic neuronal fate by repressing Ngn genes in the developing mesencephalon. Development *134*, 2783–2793.

Ovesjö, M.L., Gamstedt, M., Collin, M., and Meister, B. (2001). GABAergic nature of hypothalamic leptin target neurones in the ventromedial arcuate nucleus. J. Neuroendocrinol. *13*, 505–516.

Pak, T., Yoo, S., Miranda-Angulo, A.L., Wang, H., and Blackshaw, S. (2014). Rax-CreERT2 knock-in mice: a tool for selective and conditional gene deletion in progenitor cells and radial glia of the retina and hypothalamus. PLoS ONE *9*, e90381.

Pontecorvi, M., Goding, C.R., Richardson, W.D., and Kessaris, N. (2008). Expression of Tbx2 and Tbx3 in the developing hypothalamic-pituitary axis. Gene Expr. Patterns *8*, 411–417.

Puelles, L., Martinez-de-la-Torre, M., Bardet, S., and Rubenstein, J.L.R. (2012). Hypothalamus. In The Mouse Nervous System, C. Watson, G. Paxinos, and L. Puelles, eds. (Academic), pp. 221–312.

Quarta, C., Fisette, A., Xu, Y., Colldén, G., Legutko, B., Tseng, Y.T., Reim, A., Wierer, M., De Rosa, M.C., Klaus, V., et al. (2019). Functional identity of hypothalamic melanocortin neurons depends on Tbx3. Nat. Metab. *1*, 222–235.

Romanov, R.A., Alpár, A., Hökfelt, T., and Harkany, T. (2019). Unified classification of molecular, network, and endocrine features of hypothalamic neurons. Annu. Rev. Neurosci. *42*, 1–26.

Sanz, E., Quintana, A., Deem, J.D., Steiner, R.A., Palmiter, R.D., and McKnight, G.S. (2015). Fertility-regulating Kiss1 neurons arise from hypothalamic POMC-expressing progenitors. J. Neurosci. *35*, 5549–5556.

Saper, C.B., and Lowell, B.B. (2014). The hypothalamus. Curr. Biol. *24*, R1111–R1116.

Shi, W., Xianyu, A., Han, Z., Tang, X., Li, Z., Zhong, H., Mao, T., Huang, K., and Shi, S.H. (2017). Ontogenetic establishment of order-specific nuclear organization in the mammalian thalamus. Nat. Neurosci. *20*, 516–528.

Shimada, M., and Nakamura, T. (1973). Time of neuron origin in mouse hypothalamic nuclei. Exp. Neurol. *41*, 163–173.

Shimogori, T., Lee, D.A., Miranda-Angulo, A., Yang, Y., Wang, H., Jiang, L., Yoshida, A.C., Kataoka, A., Mashiko, H., Avetisyan, M., et al. (2010). A genomic atlas of mouse hypothalamic development. Nat. Neurosci. *13*, 767–775.

Shinoda, K., Lei, H., Yoshii, H., Nomura, M., Nagano, M., Shiba, H., Sasaki, H., Osawa, Y., Ninomiya, Y., Niwa, O., et al. (1995). Developmental defects of the ventromedial hypothalamic nucleus and pituitary gonadotroph in the Ftz-F1 disrupted mice. Dev. Dyn. *204*, 22–29.

Stuber, G.D., and Wise, R.A. (2016). Lateral hypothalamic circuits for feeding and reward. Nat. Neurosci. *19*, 198–205.

Swanson, L.W., and Sawchenko, P.E. (1983). Hypothalamic integration: organization of the paraventricular and supraoptic nuclei. Annu. Rev. Neurosci. *6*, 269–324.

Szarek, E., Cheah, P.S., Schwartz, J., and Thomas, P. (2010). Molecular genetics of the developing neuroendocrine hypothalamus. Mol. Cell. Endocrinol. *323*, 115–123.

Taniguchi, H., He, M., Wu, P., Kim, S., Paik, R., Sugino, K., Kvitsiani, D., Fu, Y., Lu, J., Lin, Y., et al. (2011). A resource of Cre driver lines for genetic targeting of GABAergic neurons in cerebral cortex. Neuron *71*, 995–1013.

Tran, P.V., Lee, M.B., Marín, O., Xu, B., Jones, K.R., Reichardt, L.F., Rubenstein, J.R., and Ingraham, H.A. (2003). Requirement of the orphan nuclear receptor SF-1 in terminal differentiation of ventromedial hypothalamic neurons. Mol. Cell. Neurosci. *22*, 441–453.

Trowe, M.O., Zhao, L., Weiss, A.C., Christoffels, V., Epstein, D.J., and Kispert, A. (2013). Inhibition of Sox2-dependent activation of Shh in the ventral diencephalon by Tbx3 is required for formation of the neurohypophysis. Development *140*, 2299–2309.

Virolainen, S.M., Achim, K., Peltopuro, P., Salminen, M., and Partanen, J. (2012). Transcriptional regulatory mechanisms underlying the GABAergic neuron fate in different diencephalic prosomeres. Development *139*, 3795–3805.

Vong, L., Ye, C., Yang, Z., Choi, B., Chua, S., Jr., and Lowell, B.B. (2011). Leptin action on GABAergic neurons prevents obesity and reduces inhibitory tone to POMC neurons. Neuron *71*, 142–154.

Wang, W., and Lufkin, T. (2000). The murine Otp homeobox gene plays an essential role in the specification of neuronal cell lineages in the developing hypothalamus. Dev. Biol. *227*, 432–449.

Weinreb, C., Rodriguez-Fraticelli, A., Camargo, F.D., and Klein, A.M. (2020). Lineage tracing on transcriptional landscapes links state to fate during differentiation. Science *367*, eaaw3381.

Wong, S.Z.H., Scott, E.P., Mu, W., Guo, X., Borgenheimer, E., Freeman, M., Ming, G.L., Wu, Q.F., Song, H., and Nakagawa, Y. (2018). In vivo clonal analysis reveals spatiotemporal regulation of thalamic nucleogenesis. PLoS Biol. *16*, e2005211.

Xie, Y., and Dorsky, R.I. (2017). Development of the hypothalamus: conservation, modification and innovation. Development *144*, 1588–1599.

Xu, Q., Tam, M., and Anderson, S.A. (2008). Fate mapping Nkx2.1-lineage cells in the mouse telencephalon. J. Comp. Neurol. *506*, 16–29.

Yee, C.L., Wang, Y., Anderson, S., Ekker, M., and Rubenstein, J.L.R. (2009). Arcuate nucleus expression of NKX2.1 and DLX and lineages expressing these transcription factors in neuropeptide Y(+), proopiomelanocortin(+), and tyrosine hydroxylase(+) neurons in neonatal and adult mice. J. Comp. Neurol. *517*, 37–50.

Zhou, X., Zhong, S., Peng, H., Liu, J., Ding, W., Sun, L., Ma, Q., Liu, Z., Chen, R., Wu, Q., and Wang, X. (2020). Cellular and molecular properties of neural progenitors in the developing mammalian hypothalamus. Nat. Commun. *11*, 4063.

Ziegler, D.R., Cullinan, W.E., and Herman, J.P. (2002). Distribution of vesicular glutamate transporter mRNA in rat hypothalamus. J. Comp. Neurol. *448*, 217–229.

Zong, H., Espinosa, J.S., Su, H.H., Muzumdar, M.D., and Luo, L. (2005). Mosaic analysis with double markers in mice. Cell *121*, 479–492.

Please cite this article in press as: Ma et al., Decoding neuronal composition and ontogeny of individual hypothalamic nuclei, Neuron (2021), https://doi.org/10.1016/j.neuron.2021.01.026

STAR★METHODS

KEY RESOURCES TABLE

REAGENT or RESOURCE	SOURCE	IDENTIFIER
Antibodies		
Rat anti-BrdU	Novus Biologicals	Cat#: NB500-169; RRID: AB_10002608
Guinea Pig anti-DLX2	(Kuwajima et al., 2006)	N/A
Guinea Pig anti-DLX1	(Lee et al., 2018)	N/A
Rabbit anti-DLX1	(Lee et al., 2018)	N/A
Chicken anti-GFP	Aves Labs	Cat#: GFP 1020; RRID: AB_10000240
Goat anti-GFP	Rockland	Cat#: 600-101-215; RRID: AB_218182
Mouse anti-NeuN	Millipore	Cat#: MAB377; RRID: AB_2298772
Rabbit anti-NKX2.1	Santa Cruz	Cat#: sc-13040; RRID: AB_793532
Rabbit anti-NPY	Peninsula Laboratories	Cat#: T-4069; RRID: AB_518503
Guinea Pig anti-OTP	Clontech	Cat#: M195
Rabbit anti-OTP	ABclonal	Cat#: A13188; RRID: AB_ 2760039
Rabbit anti-POMC	Phoenix Pharmaceuticals	Cat#: H-029-30; RRID: AB_2307442
Rabbit anti-Rax	Clontech	Cat#: M228
Rabbit anti-RFP	Rockland	Cat#: 600-401-379; RRID: AB_2209751
Goat anti-mCherry	Biorbyt	Cat#: orb11618; RRID: AB_2687829
Rabbit anti-SF1 (Nr5a1)	Cosmo Bio	Cat#: KAL-KO611
Goat anti-TBX3	Santa Cruz	Cat#: sc-17871; RRID: AB_661666
Rabbit anti-TH	Novus Biologicals	Cat#: NB300-109; RRID: AB_350437
Rabbit anti-Vimentin	Abcam	Cat#: ab92547; RRID: AB_10562134
Chemicals, peptides, and recombinant proteins		
Aqua-Mount Mounting Media	Thermo Fisher Scientific	Cat#: 13800
BrdU	Sigma	Cat#: B9285
Colchicine	Sigma	Cat#: C9754
Corn oil	Sigma	Cat#: C8267
DAPI	Thermo Fisher Scientific	Cat#: D1306; RRID: AB_2629482
Donkey serum	Millipore	Cat#: S30-100ML
Paraformaldehyde	Sigma	Cat#: P6148
Sodium tetraborate decahydrate	Sigma	Cat#: B9876
Tamoxifen	Sigma	Cat#: T5648
TFM Tissue Freezing Medium	GeneralData	Cat#: TFM-5
Sodium citrate dihydrate	Thermo Fisher Scientific	Cat#: S279
Critical commercial assays		
RNAscope® Multiplex Fluorescent Reagent Kit v2	Advanced Cell Diagnostics	Cat#: 323100
RNAscope® Probe- Mm-NPY	Advanced Cell Diagnostics	Cat#: 313321
TSA Plus Fluorescein	Akoya Biosciences	Cat#: NEL741001KT
TSA Plus Cyanine 3	Akoya Biosciences	Cat#: NEL744001KT
Experimental models: organisms/strains		
Mouse: Dlx5/6-Cre: Tg(dlx5a-cre)1Mekk/J	Jackson laboratory	008199; RRID: IMSR_JAX:008199
Mouse: Nkx2.1-Cre: C57BL/6J-Tg(Nkx2-1-cre)2Sand/J	Jackson laboratory	008661; RRID: IMSR_JAX:008661
Mouse: SST-Cre: $Sst^{tm2.1(cre)Zjh}$/J	Jackson laboratory	013044; RRID: IMSR_JAX:013044
Mouse: vGAT-Cre: B6J.129S6(FVB)-$Slc32a1^{tm2(cre)Lowl}$/MwarJ	Jackson laboratory	028862; RRID: IMSR_JAX:028862
Mouse: vGlut2-Cre: $Slc17a6^{tm2(cre)Lowl}$/J	Jackson laboratory	016963; RRID: IMSR_JAX:016963
Mouse: GAD2-Cre: $Gad2^{tm2(cre)Zjh}$/J	Jackson laboratory	010802; RRID: IMSR_JAX:010802

(*Continued on next page*)

Please cite this article in press as: Ma et al., Decoding neuronal composition and ontogeny of individual hypothalamic nuclei, Neuron (2021), https://doi.org/10.1016/j.neuron.2021.01.026

Continued

REAGENT or RESOURCE	SOURCE	IDENTIFIER
Mouse: Rax-CreER^{T2}: Rax$^{tm1.1(cre/ERT2)Sbls}$/J	Jackson laboratory	025521; RRID: IMSR_JAX:025521
Mouse: MADM11^{GT}: Igs2$^{tm1(ACTB-EGFP,-tdTomato)Luo}$/J	Jackson laboratory	013749; RRID: IMSR_JAX:013749
Mouse: MADM11^{TG}: Igs2$^{tm2(ACTB-tdTomato,-EGFP)Luo}$/J	Jackson laboratory	013751; RRID: IMSR_JAX:013751
Mouse: Rosa26$^{loxp-STOP-loxp-H2B-GFP}$	(He et al., 2012b)	N/A
Mouse: C57BL/6	Charles River	Cat#: CRL:027; RRID: IMSR_CRL:027
Software and algorithms		
Imaris	Bitplane	https://imaris.oxinst.com/packages
SigmaPlot 13.0	Systat Software	https://systatsoftware.com/
GraphPad Prism 8	GraphPad Software	https://www.graphpad.com:443/
Photoshop CS6	Adobe	https://www.adobe.com/
Heatmapper	(Babicki et al., 2016)	http://www1.heatmapper.ca/
Seurat	(Butler et al., 2018)	https://satijalab.org/seurat/

RESOURCE AVAILABILITY

Lead contact

Further information and requests for resources and reagents should be directed to and will be fulfilled by the Lead Contact, Hongjun Song (shongjun@pennmedicine.upenn.edu).

Material availability

No new unique reagents were generated in the current study.

Data and code availability

Software used in this study is listed in the key resources table. There is no custom code used in the current study.

EXPERIMENTAL MODEL AND SUBJECT DETAILS

Animals

Animals were housed in temperature and humidity-controlled facilities under 14 hour light/10 hour dark cycle and with food and water *ad libitum*. All transgenic mice used in this study were maintained on the C57BL/6 background. The wild-type C57BL/6 mice were purchased from Charles River. The time of pregnancy was determined by the presence of a vaginal plug (E0.5). The day of birth was designated as postnatal day 0 (P0). Both male and female mice were used for all experiments, and no obvious sex differences were observed. All animal procedures used in this study were performed in compliance with protocols approved by the Institutional Animal Care and Use Committee of University of Pennsylvania.

The source and information of all genetically modified mice are listed in the Key resources table. *DLX5/6-Cre*, *NKX2.1-Cre*, *SST-Cre*, *vGlut2-Cre*, *vGAT-Cre* and *GAD2-Cre* mice were crossed with *Rosa26$^{loxp-STOP-loxp-H2B-GFP}$* (referred to as *H2B-GFP*) reporter mice to obtain the *DLX5/6-Cre:H2B-GFP, NKX2.1-Cre:H2B-GFP, SST-Cre:H2B-GFP, vGlut2-Cre:H2B-GFP, vGAT-Cre:H2B-GFP and GAD2-Cre:H2B-GFP* mice, respectively. It is important to note that we combined endogenous protein expression and transgenic mouse lines based on Cre recombinase to label neurons of the hypothalamic nuclei. Considering the potential downregulation and post-transcriptional regulation of gene expression, the Cre-dependent GFP expression may not reflect the endogenous gene and protein expression. Indeed, we found different levels of downregulation of DLX1 and DLX2 expression in DLX5/6-Cre lineage cells (Figure S1A), and downregulation of NKX2.1 expression in NKX2.1-Cre lineage cells (Figures 6C and 6D).

Rax-CreER$^{T2+/-}$ mice were crossed with *H2B-GFP* mice to obtain the *Rax-CreER$^{T2+/-}$:H2B-GFP* (referred to as *Rax-CreER^{T2}:H2B-GFP*) mice. To establish the MADM labeling system, *Rax-CreER$^{T2+/-}$* mice were crossed with *MADM11$^{GT/GT}$* mice to generate *Rax-CreER$^{T2+/-}$:MADM11$^{GT/-}$* mice. The *Rax-CreER$^{T2+/-}$:MADM11$^{GT/-}$* mice were then backcrossed with *MADM11$^{GT/GT}$* mice to obtain *Rax-CreER$^{T2+/-}$:MADM11$^{GT/GT}$* mice. Finally, *Rax-CreER$^{T2+/-}$:MADM11$^{GT/GT}$* mice were crossed with *MADM11$^{TG/TG}$* mice to harvest the *Rax-CreER$^{T2+/-}$:MADM11$^{GT/TG}$* mice (referred to as *Rax-CreER^{T2}:MADM$^{GT/TG}$*).

METHOD DETAILS

BrdU and Tamoxifen Treatments

BrdU (Bromodeoxyuridine) pulse labeling was used to analyze the birth-dating of neurons in the Arc, VMH and TuN. A stock solution of BrdU (10 mg/ml, Sigma, B9285) was made in saline solution (0.9%). A single injection of BrdU (50 mg/kg, body weight) was

administered intraperitoneally to the timed pregnant *DLX5/6-Cre:H2B-GFP* female mice at E9.5, E10.5, E11.5, E12.5, E13.5, E14.5, or E15.5. Mice were perfused at P21.

Tamoxifen treatment was used to activate Cre-ER in *Rax-CreER^{T2}* mice. Stock solutions of tamoxifen (66.67 mg/mL, Sigma, T5648) were prepared in a mixture (5:1) of corn oil and ethanol with 37°C water bath and occasional vortexing, and were aliquoted and stored at −20°C (Berg et al., 2019). For the fate-mapping study using *Rax-CreER^{T2}:H2B-GFP* mice, timed pregnant females (E9.5) received a single intraperitoneal injection of tamoxifen (120 μg/g body weight), and embryos were examined at E13.5. The MADM system based on Cre-mediated interchromosomal recombination is a very sparse labeling system that requires a high dose of tamoxifen for induction (Hippenmeyer et al., 2010; Llorca et al., 2019). To achieve very sparse labeling using the *Rax-CreER^{T2}:MADM$^{GT/TG}$* system for clonal analysis, we first tested different tamoxifen injection doses. Tamoxifen was administered intraperitoneally to the timed pregnant females at E9.5 and embryos were analyzed at E11.5/E12.5. No labeled progenitors were found (n > 30; hypothalamic hemispheres) with doses of 40 μg/g and 60 μg/g (body weight). At the dose of 120 μg/g (body weight), a considerable number of hypothalamic hemispheres with sparsely labeled progenitors was observed. To achieve sparse labeling and also avoid severe embryonic lethality, we used tamoxifen injection doses at a range of 120-160 μg/g (body weight). Therefore, although the high doses of tamoxifen have a relatively long half-life, the high threshold for induction of the MADM system makes induction after three days highly unlikely to affect lineage analysis. For short-term lineage tracing, tamoxifen was administered at E9.5 and embryos were dissected at E11.5 or E12.5. For long-term lineage tracing, tamoxifen was administered at E9.5 and embryos were dissected at the expected delivery date (E19.5, referred to as P0) because tamoxifen treatment caused dystocia.

Brain Tissue Preparation and Sectioning

Mice were anesthetized with isoflurane and then transcardially perfused with DPBS followed by 4% paraformaldehyde (PFA) in PBS. For embryonic samples, timed pregnant females were euthanized by cervical dislocation, and embryos were euthanized by decapitation before dissection. Brains were dissected and post-fixed in 4% PFA at 4°C, and then cryoprotected in 30% sucrose solution overnight at 4°C. All brains were embedded in tissue freezing medium (GeneralData, TFM-5), and stored at −80°C before sectioning.

Coronal brain sections (30 μm for P21 and P28 samples, 40-50 μm for embryonic and P0 samples) were prepared with a cryostat (Leica, CM3050S). Sections were collected on Superfrost Plus Microscope Slides (Thermo Fisher Scientific, 12-550-15), and serial sections were collected for clonal analysis. Brain sections on slides were stored at −20°C before immunostaining.

Immunohistology, Confocal Imaging and Counting

Brain sections on slides were washed in TBS, blocked and permeabilized with blocking solution (5% normal donkey serum and 0.1% Triton X-100 in TBS) for 2 hours at room temperature. Brain sections were then incubated with primary antibodies in blocking solution for ~48 hours at 4°C. After washing in TBS, brain sections were incubated with secondary antibodies (Jackson ImmunoResearch) and DAPI (Thermo Fisher Scientific) in blocking solution for 2 hours at room temperature. Sections were then washed in TBS and mounted with mounting media (Aqua-Mount, Thermo Fisher Scientific, 13800). All primary antibodies used in this study are listed in the Key resources table. Secondary antibodies (Cy2 or Alexa Fluor 488, Cy3 or Alexa Fluor 555, Cy5 or Alexa Fluor 647, Jackson ImmunoResearch) were used at a dilution of 1:400. In clonal analysis studies, the primary antibodies against GFP and tdTomato, and the corresponding secondary antibodies were used at a dilution of 1:2000.

Images were acquired with Zeiss LSM 710 or Zeiss LSM 810 confocal microscopes with 10X, 20X and 25X objectives. Images were analyzed using Imaris and Adobe Photoshop software. Brightness and contrast of entire images were adjusted as necessary for visualization. For cell counting, Tile Scan model was used to cover the corresponding nuclei. Five Z sections with 1 μm intervals (4 μm thick) were collected with Z stack Acquisition model. Maximum Intensity Projection of five Z sections were exported as TIFF format images. Cells were manually counted using Count Tool of Adobe Photoshop (Adobe Photoshop CS6). For all counting, the specific marker positive cells of the entire Arc, VMH or TuN nucleus in each section were counted, and DAPI was used to identify the cell nuclei. For each section, the integrated fluorescence intensity of each individual channel was measured in marker-negative cells and the positivity threshold was set at three times this value. For counting GFP$^+$ neurons from H2B-GFP mice, and TBX3$^+$, OTP$^+$, DLX1$^+$, DLX2$^+$, NKX2.1$^+$ and SF1$^+$ neurons, a positive signal with nuclear morphology and DAPI$^+$ nucleus was identified as a GFP$^+$ neuron and TF$^+$ neuron. For counting POMC$^+$, NPY$^+$ and TH$^+$ neurons, a positive signal with cell body morphology and DAPI$^+$ nucleus was recognized as a positive neuron. Because of the high sensitivity and specificity of RNAscope fluorescent *in situ* hybridization, neurons with punctate NPY^{mRNA+} signals surrounding the DAPI$^+$ nuclei were identified as NPY^{mRNA+} neurons.

Antigen Retrieval Treatment

Antigen retrieval was performed for DLX2 and BrdU staining. Brain sections immunostained for DLX2 underwent antigen retrieval with Sodium Citrate Buffer (10 mM Sodium citrate, 0.05% Tween 20, pH 6.0). Sodium Citrate Buffer with brain sections on slides were heated to 100°C, and were cooled down for one hour at room temperature. After washing in TBS, brain sections were immunostained with standard protocols. Brain sections stained for BrdU underwent antigen retrieval with HCl solution (2N HCl). Brain sections on slides were incubated in HCl solution for one hour at room temperature, and then washed in sodium borate buffer (0.1M sodium tetraborate decahydrate, pH 8.5; 2X10 minutes). After washing in TBS, brain sections were immunostained with standard protocols.

Please cite this article in press as: Ma et al., Decoding neuronal composition and ontogeny of individual hypothalamic nuclei, Neuron (2021), https://doi.org/10.1016/j.neuron.2021.01.026

In Situ Hybridization

Coronal brain sections (30 μm) were prepared with a cryostat (Leica, CM3050S) and collected in wells of 24-well tissue culture plates. *In situ* hybridization was performed using the RNAscope Multiplex Fluorescent Kits (323100) according to the manufacturer's instructions (Advanced Cell Diagnostics). In brief, brain sections were first pre-treated with hydrogen peroxide for 10 minutes at room temperature, then with protease III for 20 minutes at 40°C. After the pre-treatment steps, brain sections were incubated with NPY probes (RNAscope Probe-Mm-NPY, 313321) for 2 hours at 40°C and the standard RNAscope protocol was followed. TSA Plus Fluorescein (Akoya Biosciences, NEL741001KT) and TSA Plus Cyanine 3 (Akoya Biosciences, NEL744001KT) were used for color reactions. After washes, brain sections were immunostained for GFP, TBX3 and OTP using the standard procedure described above.

Single-cell RNA Sequencing Analysis

Single-cell RNA seq dataset of the adult mouse ARC was retrieved from a public repository (Campbell et al., 2017). Seurat v2.3.4 was used to analyze the single-cell RNA-seq data (Butler et al., 2018). Standard pre-processing pipelines, including normalization and scaling, were followed without additional modifications. Clustering and tSNE dimensionality reduction were performed based on empirically selected PCs (Figure S2J). For further analysis, neuronal cell clusters were identified based on enriched expression of neuronal markers SYT1 and SNAP25, and expression of selected genes in neuronal populations was generated using the DoHeatmap function (Figure S2K).

MADM-based Clonal Lineage Analyses

In the $MADM^{GT/TG}$ system, G2-recombination in dividing progenitors followed by X segregation (G_2-X event) reconstitutes only green GFP or red tdTomato fluorescent marker in each daughter cell, resulting in permanent tracing of the two daughter cells and their descendent lineages (Figure S5A). In addition, G_2-recombination followed by Z segregation (G_2-Z event), G_1, or G_0 recombination events leads to simultaneous expression of the reconstituted GFP and tdTomato in the same cell, resulting in yellow lineages (Figure S5A). It is important to note that our single-cell lineage analysis in this work takes advantage of G_2-X events during cell division in the MADM system, but lineages of quiescent progenitors were not explicitly examined. Therefore, we cannot rule out the possibility that some quiescent progenitors in the pArc and pVMH at E9.5 could give rise to fate-restricted lineages later (Llorca et al., 2019).

For short-term (E9.5-E11.5/E12.5) clonal analysis using the *Rax-CreER^{T2}:MADM$^{GT/TG}$* system, expression of GFP and tdTomato without immunostaining was not strong enough to be observed in all fluorescent protein-containing cells under a fluorescence microscope. Serial sections of all brains were immunostained with GFP, tdTomato and a third marker (TBX3, OTP, or SF1), and counterstained with DAPI. Serial sections were then checked under a fluorescence microscope after staining. The hypothalamic hemispheres without any Green/Red (G/R) or Yellow (Y) clones were not imaged, but the number of the hemispheres was recorded. The median eminence and pituitary stalk (infundibulum) were excluded from our study because of poor neuron production. For the hypothalamic hemispheres containing labeled clones (G/R and/or Y) cells, images of serial sections from the first section containing labeled cell/cells to the last section containing labeled cell/cells were collected. The percentages of hemispheres containing one clone, two or more clones, or no clones were quantified. Only Green/Red clones from G2-X events were analyzed to investigate the features of individual hypothalamic progenitors. The RGPs of the hypothalamus were identified by a combination of the location (ventricular zone) and morphology (apical and radial processes). The division patterns of the individual hypothalamic RGPs were examined in detail.

For long-term (E9.5-P0) lineage analysis using the *Rax-CreER^{T2}:MADM$^{GT/TG}$* system, serial sections on slides were checked under a fluorescence microscope before immunostaining. All yellow clones were excluded from further analysis, and only Green/Red clones were used for individual lineage analysis. We reasoned that either the RGP^G or RGP^R lineage from the last symmetric division of the G2-X event represents a complete lineage of an individual hypothalamic RGP (Figure 5C). However, considering depleted RGP^G and RGP^R in some clones and the existence of clones with more than one persistent $RGPs^G$ or $RGPs^R$ resulting from symmetric division of RGP^G or RGP^R, we defined the "complete individual RGP^G (or RGP^R) lineage" from the speculated symmetric division of the G2-X event as the following: the RGP^G (or RGP^R) lineage with only one retained RGP^G (or RGP^R) contains certain differentiated cells, and the RGP^G (or RGP^R) lineage without RGP^G (or RGP^R) contains more than two differentiated cells (Figure 5C). In addition, the whole clone (including both green and red cells) from the speculated asymmetric division of the G2-X event also represents a complete lineage of an individual RGP. Given that the RGP^G and RGP^R lineages are equipotent in principle in the $MADM^{GT/TG}$ system, we only used the defined "complete individual RGP^G lineages" from the speculated symmetric division of G2-X events to analyze the individual pArc lineages (Figure 5C). The numbers of the green neurons, red neurons and retained RGPs were analyzed to find the "complete individual RGP^G lineages" from the speculated symmetric division of G2-X event. Then the locations (Arc, VMH-TuN, or other areas) of the lineages were estimated, and the lineage analysis was performed according to the locations of the lineages. The median eminence and pituitary stalk (infundibulum) were excluded from our study because of poor neuron production. If both Arc and VMH-TuN lineages were found in the same brain (either in different hemispheres or in the same hemisphere), the brain sections were used to analyze the Arc lineages because the Arc lineages were difficult to collect due to the small area of pArc.

For brain sections with estimated individual RGP^G lineages in the Arc, serial sections were immunostained with GFP, TBX3, OTP and DLX1 using the Staining/Restaining protocols (see details in the Restaining protocols below). The location of RGP^G/RGP^R progenitors (if existing) in the pArc was confirmed by TBX3 expression domain. The lineages with RGP^G/RGP^R progenitors located outside of the pArc domain (e.g., pVMH) were excluded from further analysis. Because all neurons of individual pArc lineages

Please cite this article in press as: Ma et al., Decoding neuronal composition and ontogeny of individual hypothalamic nuclei, Neuron (2021), https://doi.org/10.1016/j.neuron.2021.01.026

with RGPs were restricted in the Arc, which suggested pArc progenitors only generate the Arc neurons, we also recognized lineages without RGP^G/RGP^R progenitors (RGP depleted clones) but restricted in the Arc as pArc lineages. After identified as individual pArc lineages, the Arc1-4 subpopulations of all neurons from individual RGP^G lineages were analyzed and quantified.

For the brain sections with estimated individual RGP^G lineages in the VMH-TuN, the serial sections were immunostained with GFP (Cy2), NKX2.1 (Cy3), OTP (Cy5), and also counterstained with DAPI. The VMH-TuN subareas $VMH_{dm/c}$, VMH_{vl} and TuN were delineated by coordinating NKX2.1 expression level, OTP expression and DAPI. The location of RGP^G/RGP^R progenitors (if existing) in the pVMH was confirmed by NKX2.1 expression in the ventricular zone and VMH. The lineages with RGP^G/RGP^R progenitors located outside of the pVMH domain (e.g., subparaventricular area or paraventricular area) were excluded from further analysis. Because all neurons of individual pVMH lineages with RGPs were restricted in the VMH-TuN, which suggested pVMH progenitors only generate the VMH-TuN neurons, we also recognized lineages without RGP^G/RGP^R progenitors (depleted clones) but restricted in the VMH-TuN as pVMH lineages. After identified as individual pVMH lineages, the distribution of all neurons from individual RGP^G lineages in the VMH-TuN subareas $VMH_{dm/c}$, VMH_{vl} and TuN was analyzed and quantified. Because only GFP^+ cells from the RGP^G lineages were used to perform lineage analysis, the red tdTomato$^+$ cells from RGP^R lineages can be neglected during the staining, or stained using the same Cy3 channel with NKX2.1. The red tdTomato$^+$ cells not stained with antibodies (processes cannot be recognized) were difficult to distinguish from the NKX2.1-Cy3 (also red) cells after staining. The red tdTomato$^+$ cells stained with antibodies (tdTomato-Cy3, processes can be recognized) can be distinguished from the NKX2.1-Cy3 (also red) cells after staining.

Staining/Restaining Protocol

To identify four Arc1-4 subpopulations with TBX3, OTP and DLX combinations in long-term (E9.5-P0) individual RGP^G lineages, and to overcome the limitations of available color channels and antibody species, the following restaining method was used (Figure S5H). DLX1 antibody (Rabbit) was used to label DLX-lineage cells. Serial brain sections on slides were checked under a fluorescence microscope to identify the "complete individual RGP^G lineages" before immunostaining. After the individual RGP^G lineages in the Arc were identified, serial sections on slides were simultaneously immunostained with GFP (Chicken; Cy2), TBX3 (Goat; Cy3) and OTP (Guinea Pig; Cy5), and also counterstained with DAPI using standard immunostaining protocols (first round of staining). Images of the sections (GFP-Cy2, TBX3-Cy3, OTP-Cy5 and DAPI) were collected by confocal microscope (first set of images). Through the Staining/Imaging step, TBX3 and OTP expression in GFP^+ cells were obtained, which cannot be affected by the following Restaining step. Because the OTP^+ neurons and $DLX1^+$ neurons were mutually exclusive populations, the GFP^+/OTP^+ cells were recognized as $GFP^+/OTP^+/(DLX1^-)$ cells and excluded from further DLX1 expression analysis, and the following DLX1-restaining can share the same color channel with OTP staining. Coverslips were removed carefully and sections on the slides were washed in TBS. Sections on slides were then immunostained with DLX1 (Rabbit; Cy5, the same color channel with OTP) using standard immunostaining protocols (secondary round of staining, restaining). Images of the sections (GFP-Cy2, TBX3-Cy3, OTP-DLX1-Cy5 and DAPI) were collected again by confocal microscope (second set of images). Through the Restaining/Imaging step, DLX1 expression in GFP^+/OTP^- cells was obtained. After Staining/Restaining, TBX3, OTP and DLX1 expression in GFP^+ cells was obtained. Thus, four Arc1-4 subtypes can be identified within individual RGP^G lineages. The reliability of DLX1-restaining was validated by comparing the Staining/Restaining of DLX1-Guinea Pig/DLX1-Rabbit with the normal double staining of DLX1-Guinea Pig and DLX1-Rabbit, both of which showed complete overlap of $DLX1^+$-Guinea Pig neurons and $DLX1^+$-Rabbit neurons (100%; n = 4; P0). The reliability of DLX1-restaining was also validated by comparing the Staining/Restaining of OTP-Guinea Pig/DLX1-Rabbit with the normal double staining of OTP-Guinea Pig and DLX1-Rabbit, both of which showed non-overlapping OTP^+-Guinea Pig neurons and $DLX1^+$-Rabbit neurons (normal staining/restaining: OTP^+ neurons expressing DLX1, $< 1\%/< 1\%$; $DLX1^+$ neurons expressing OTP, $< 2\%/< 2\%$; n = 4; P0). Because only GFP^+ cells from the RGP^G lineages were used to perform lineage analysis, the red tdTomato$^+$ cells from the RGP^R lineages can be neglected during the staining and restaining, or immunostained using the same Cy3 channel with TBX3. The red tdTomato$^+$ cells without immunostaining with antibodies (processes cannot be recognized) were difficult to distinguish from the TBX3-Cy3 (also red) cells after staining and restaining (Figure 5D). The red tdTomato$^+$ cells immunostained with antibodies (tdTomato-Cy3, processes can be recognized) can be distinguished from the TBX3-Cy3 (also red) cells after staining and restaining (Figure S5I).

QUANTIFICATION AND STATISTICAL ANALYSIS

All sample sizes and ages of the mice are indicated in the figure legends and text. All values are shown as mean ± SEM or mean, which are annotated in the figure legends. Statistical analyses were performed using SigmaPlot 13.0, GraphPad Prism 8, Microsoft Excel and Heatmapper (Babicki et al., 2016). In all population-level studies, hypothalamic hemispheres from different mice and several brain sections (3-4 sections for E15.5 and P0; 4-5 sections for P21 and P28) across rostro-caudal levels of specific nuclei were quantified.

For counting of the Arc, VMH and TuN neurons at P21 and P28, every sixth section (30 μm) was processed for different marker staining. After staining, 4-5 sections across the rostro-caudal levels from approximately bregma −1.58 mm to bregma −2.30 mm were selected for counting the Arc neurons. 4-5 sections across the rostro-caudal levels from approximately bregma −1.34 mm to bregma −2.06 mm were selected for counting the VMH and TuN neurons. For counting of the Arc, VMH and TuN neurons at P0, every fourth section (40 μm) was processed for different markers staining. After staining, 4 sections across the rostro-caudal levels of the Arc, VMH or TuN were selected for counting the neurons. For counting of the Arc neurons at E15.5, every third section

Please cite this article in press as: Ma et al., Decoding neuronal composition and ontogeny of individual hypothalamic nuclei, Neuron (2021), https://doi.org/10.1016/j.neuron.2021.01.026

(40-50 μm) was processed for staining of different markers. After staining, 3-4 sections across the rostro-caudal levels of the Arc were selected for counting the Arc neurons. Sections of different animals were selected from the similar rostro-caudal levels. All cells within a given nucleus were counted in each section for quantification. To delineate Arc1-7 subpopulations with TBX3, OTP, and DLX^{GFP} combinations at P28, 15 sections with 245-484 cells per section from three hypothalamic hemispheres were examined. To delineate Arc1-7 subpopulations with TBX3, OTP, and DLX2 combinations at P28, 15 sections with 373-509 cells per section from three hypothalamic hemispheres were examined. To identify TuN1-3 subpopulations with OTP and DLX^{GFP} combinations at P28, 15 sections with 125-349 cells per section from three hypothalamic hemispheres were examined. To identify the VMH neurons ($NeuN^+$) expressing SF1, 15 sections with 434-1370 cells per section from three hypothalamic hemispheres were examined. To identify the VMH neurons ($NeuN^+$) expressing NKX2.1, 15 sections with 753-1400 cells per section from three hypothalamic hemispheres were examined. The percentage of each hypothalamic hemisphere was obtained first, and then the mean of percentages from three or four hypothalamic hemispheres (n = 3 or 4) was obtained. The percentage values are shown as mean ± SEM or mean in the text and Figures.

Quantification of Population-Level Analyses

To overcome the limitation of available color channels, the following unusual staining methods were performed. To analyze all Arc neurons expressing TFs, we simultaneously immunostained NeuN, TBX3, OTP, and DLX^{GFP} with OTP and DLX^{GFP} sharing the same Cy2 channel (NeuN-Cy3, TBX3-Cy5, OTP-DLX^{GFP}-Cy2). $NeuN^+/TBX3^+/OTP^+$-DLX^{GFP+} neurons among total $NeuN^+$ neurons were quantified (Figure 1D). To analyze the relationship between the POMC neurons and Arc1 ($TBX3^+/OTP^-/DLX^{GFP-}$) neurons, we simultaneously immunostained POMC, TBX3, OTP, and DLX^{GFP} with OTP and DLX^{GFP} sharing the same Cy2 channel (POMC-Cy5, TBX3-Cy3, OTP-DLX^{GFP}-Cy2). $POMC^+/TBX3^+/OTP^-$-DLX^{GFP-} neurons among total $POMC^+$ neurons or among total $TBX3^+/OTP^-$-DLX^{GFP-} (Arc1) neurons were quantified (Figure 2B).

For quantifications regarding VMH and TuN neurons, delineation of boundaries was summarized as following with DAPI counterstaining used for all counting. The boundary between VMH and Arc was delineated by coordinating high density of $NKX2.1^+$ cells in VMH and high density of OTP^+ or DLX^{GFP+} cells in Arc. The boundary between VMH and LHA was delineated by coordinating high density of $NKX2.1^+$ cells in VMH and high density of OTP^+ or DLX^{GFP+} cells in LHA. The boundary between $VMH_{dm/c}$ and VMH_{vl} was delineated by coordinating weak expression of NKX2.1 in $VMH_{dm/c}$ cells and high expression NKX2.1 in VMH_{vl} cells, and comparing sections with the similar SF1 stained sections. The boundary between TuN and LHA was delineated by the existence of many OTP^+/DLX^{GFP+} cells in TuN but not LHA, and comparing sections with the similar sections from *NKX2.1-Cre:H2B-GFP* mice and *vGlut2-Cre:H2B-GFP* mice.

BrdU Birth-Dating Analysis

A single pulse of BrdU was intraperitoneally injected into the timed pregnant *DLX5/6-Cre:H2B-GFP* female mice (at E9.5, E10.5, E11.5, E12.5, E13.5, E14.5, or E15.5). Birth-dating analysis of the Arc, VMH and TuN neurons was performed at P21. For birth-dating analysis of Arc neurons, $BrdU^+/OTP^+$ neurons among total OTP^+ neurons were quantified to analyze the birth-dating of Arc2 ($TBX3^+/OTP^+/DLX^{GFP-}$) neurons because nearly all OTP^+ neurons expressed TBX3, but rare OTP^+ neurons express DLX^{GFP} in the Arc. $BrdU^+/TBX3^+/DLX^{GFP+}$ neurons among total $TBX3^+/DLX^{GFP+}$ neurons were quantified to analyze the birth-dating of Arc3 ($TBX3^+/OTP^-/DLX^{GFP+}$) neurons because rare DLX^{GFP+} neurons expressed OTP in the Arc. $BrdU^+/TBX3^-/DLX^{GFP+}$ neurons among total $TBX3^-/DLX^{GFP+}$ neurons were quantified to analyze the birth-dating of Arc4 ($TBX3^-/OTP^-/DLX^{GFP+}$) neurons because rare DLX^{GFP+} neurons expressed OTP in the Arc. We simultaneously stained BrdU, TBX3, OTP, and DLX^{GFP} with OTP and DLX^{GFP} sharing the same Cy2 channel (BrdU-Cy3, TBX3-Cy5, OTP-DLX^{GFP}-Cy2) (Figure 4D). $BrdU^+/TBX3^+/OTP^-$-DLX^{GFP-} neurons among total $TBX3^+/OTP^-$-DLX^{GFP-} neurons were quantified to analyze the birth-dating of Arc1 ($TBX3^+/OTP^-/DLX^{GFP-}$) neurons (Figure 4E).

For birth-dating analysis of the $VMH_{dm/c}$ and VMH_{vl} neurons, $BrdU^+/NKX2.1^+$ neurons among total $NKX2.1^+$ neurons of $VMH_{dm/c}$, and $BrdU^+/NKX2.1^+$ neurons among total $NKX2.1^+$ neurons of VMH_{vl} were quantified. For birth-dating analysis of the TuN neurons, $BrdU^+/TFs^+$ (OTP^+ and/or DLX^{GFP+}) neurons among total TFs^+ (OTP^+ and/or DLX^{GFP+}) neurons were quantified (Figures 6H, S6E, and S6F).